THE GEOLOGICAL SOCIETY OF AMERICA®

Lithium isotopes of the Peace River Arch in the Western Canada Sedimentary Basin: A framework for resolving deep basin lithium sources

Cody N. Lazowski[1,†], Boriana Kalderon-Asael[2], Dan Asael[2], Maria L. Arizaleta[1], Scott Melnyk[1], Sasha Wilson[1], Daniel S. Alessi[1], Noah J. Planavsky[2], Kurt O. Konhauser[1], and Murray K. Gingras[1]

[1]*Department of Earth and Atmospheric Sciences, University of Alberta, Edmonton, Alberta T6G 2E3, Canada*

[2]*Department of Earth and Planetary Sciences, Yale University, New Haven, Connecticut 06511, USA*

ABSTRACT

Lithium (Li) enrichment in the formational brines of deep sedimentary basins has emerged as a crucial component of global Li inventories. However, the processes driving the formation of Li brines remain poorly understood. Here we use lithofacies analysis and Li isotope geochemistry to investigate the sources and emplacement mechanisms within weathered subcropping units and overlying detrital sediments of the Peace River Arch (PRA) in the Western Canada Sedimentary Basin (WCSB). We analyze data from three drill cores that traverse Precambrian basement and five of its overlying siliciclastic and carbonate units. These cores reside both within and outside of the fault zone proposed as a migration pathway for hydrothermal emplacement. Lithofacies analysis revealed that these sediments were weathered directly from crystalline basement of the cratonic uplift and transported via a fluvial-deltaic system into the surrounding shallow marine basin. Like modern weathering regimes, we find Li concentrations are strongly lithofacies dependent, ranging from 0.4 ppm to 167.3 ppm, with δ^7Li values ranging from 1.5‰ to 23.5‰. Our results show that superficially weathered, coarse-grained lithologies and carbonate facies are Li-depleted and δ^7Li-enriched, whereas fine-grained facies characterized by the formation of secondary clay minerals are δ^7Li-depleted and exhibit the highest Li concentrations. Contrary to the prevailing model of hydrothermal emplacement, we find no visual, mineralogical, or geochemical evidence of hydrothermal alteration. Instead, Li enrichment is attributed to weathering of the crystalline basement and syndepositional emplacement during basin evolution. Sedimentation continued throughout the overall transgression of the Devonian, resulting in the interfingering of these clastics with every onlapping unit until the PRA was buried at the end of the Devonian. This study is the first to directly trace Li from source to sink in an ancient sedimentary basin, and we show that the modern distribution of Li brine concentrations can be explained by their proximity and intercalation with weathered subcropping units. Moreover, our results provide a source and mechanism of transporting dissolved Li into the restricted basin, supporting previous suggestions that Li brines toward the southeastern portion of the WCSB are the result of basin scale evaporation-concentration of paleoseawater. Our results underscore the link between the nature and distribution of basin fill sediments and the formation of Li-enriched brines. As formational brines gain prominence as future Li resources, the methodology presented here establishes a framework for characterizing Li genesis, with applications for sedimentary basins worldwide.

INTRODUCTION

Lithium (Li) is a widely used, critical element in many modern materials and technologies. It is used in the production of ultra-low expansion glasses and ceramics for applications ranging from stove tops to high performance optics, as well as Li-based lubricants for heavy machinery and critical aircraft components (Bibienne et al., 2020). Its most extensive use, however, is in the ever-accelerating development of energy storage technologies, which accounts for an estimated 80% of global Li end-use (Ambrose and Kendall, 2020; USGS, 2023). Annual Li production increased from 38 to 130 kilotons between 2016 and 2022 and is forecast to reach 380 kilotons by 2028 (Bibienne et al., 2020; USGS, 2023). Currently recognized resources total an estimated 98 million tons and include hard rock (pegmatites and granites), Li brines (continental and deep-groundwater brines), and Li-bearing clay minerals (e.g., hectorite, $M_y^+Mg_{3-y}Li_ySi_4O_{10}(OH)_2{\cdot}nH_2O$, illite, and other Li-bearing smectites; Bowell et al., 2020; USGS, 2023). Although these resources far exceed projected demand for the foreseeable future, over 90% of global production is currently dominated by pegmatite mining in Australia, brine extraction in Chile and Argentina, and both hard rock and brine operations in China (USGS, 2023). With increasing environmental and geopolitical uncertainty surrounding the current supply chain, evaluating domestic resources has become a primary goal for government and manufacturers alike (Murdock et al., 2021; Benson et al., 2017).

To satisfy these demands, alternative Li resources, such as deep formational brines, are increasingly gaining attention. Groundwaters within ancient sedimentary basins have long been recognized as potential resources owing to their unusually high concentrations of dissolved metals and global distributions (Kharaka and Hanor, 2003). Formational brines hosting Li have been identified in 48 sedimentary basins across six continents, with concentrations ranging from <0.001 mg/L to 1800 mg/L (Dugamin et al., 2021). Preliminary estimates from just five of these basins—Appalachian Basin (Oriskany and Medina), Salton Trough (Salton Sea), North Louisiana Basin (Atlanta), Rhine Graben (Landau) and the Western Canada Sedimentary Basin (Swan Hills, Leduc, and Basal Quartz)—indicate that, with concentrations ranging from 15.0 mg/L to 277 mg/L, collectively they contain Li resources comparable to currently exploited salars and hard rock mines and will likely represent major contributors to the future supply chain (Dugamin et al., 2021). Deep formational waters are already produced in excess during oil, gas, and low enthalpy geothermal operations

Cody N. Lazowski https://orcid.org/0000-0002-1936-1311

[†]lazowski@ualberta.ca

GSA Bulletin; November/December 2025; v. 137; no. 11/12; p. 4993–5008; https://doi.org/10.1130/B38102.1.
Published online 9 June 2025

around the world, and their expected production in geologic carbon sequestration make them an accessible and desirable target for secondary resource evaluation (Maloney and Yoxtheimer, 2012; Breunig et al., 2013; Lund and Toth, 2021; Marza et al., 2024).

Although Li enrichment has been widely documented in deep sedimentary basins, the nature of its emplacement remains understudied. In near surface or surface brines, Li can more readily be traced from source to sink by analyzing nearby sediments, bedrock, magmatic-hydrothermal systems, or hydrologic flow into the basin (e.g., Araoka et al., 2014; Benson et al., 2017; Godfrey and Álvarez-Amado, 2020; Coffey et al., 2021). However, owing to the relative inaccessibility and limited availability of ancient, deep basin data compared to modern and near modern systems, most explanations for the development of deep formational brines involve some combination of late-stage seawater evaporation, complex water-rock interactions, meteoric water mixing, or hydrothermal influx (e.g., Connolly et al., 1990a, 1990b; Elders and Cohen, 1983; Wilson and Long, 1993; Stueber et al., 1993; Tesmer et al., 2007; Sanjuan et al., 2022). Moreover, it is not always clear whether the emplacement of metals is the result of syndepositional or post-depositional processes, hindering the ability to characterize potential resources and understand their distributions. As such, without a clearer understanding of the source of Li to these basins, it becomes difficult to elucidate the precise mechanisms responsible for its enrichment in their brines.

The Western Canada Sedimentary Basin (WCSB) is an archetype of these challenges, with >500 Ma of sediments preserving a complex history of transgressive-regressive sequences, tectonic uplift, subsidence, and continental accretion (Porter et al., 1982). Here, brines of economic interest are documented within Paleozoic sediments of Alberta and Saskatchewan, but the source to these brines and timing of their emplacement remains elusive. Groundwaters hosting Li concentrations up to 57 mg/L and 190 mg/L are recognized in the Devonian aged Winnipegosis and Duperow Formations of southern Saskatchewan, respectively (Jensen, 2015, 2016). Within the Alberta basin, concentrations up to 115 mg/L, 130 mg/L, and 140 mg/L are recognized in Devonian carbonates of the Wabamun, Beaverhill Lake, and Woodbend Groups, respectively (Hitchon et al., 1993). A previous investigation noted that in the western portion of the Alberta basin, elevated Li concentrations correlate with increased radiogenic $^{87}Sr/^{86}Sr$ levels and commonly occur within dolomitized carbonates (Eccles and Berhane, 2011). Those authors suggest that Li enrichment may have resulted from either (1) direct contact between Devonian seawater and the basement or (2) an influx of hydrothermal fluids mobilized from the basement via fault and fracture systems, which migrated along the overlying siliciclastics and upward into carbonate units (Eccles and Berhane, 2011). Ultimately, Eccles and Berhane (2011) favored a hydrothermal model in which Li emplacement was a post-depositional process that may have been associated with the Laramide Orogeny as late as the Cretaceous, although they acknowledged this hypothesis to be highly speculative. Eastward into the central and southern Alberta basin, an analysis of stable hydrogen and oxygen isotopes suggests these brines originally formed through evaporation-concentration of seawater, and that the Li was later emplaced by the dissolution of in situ Li-bearing evaporitic minerals (i.e., carnallite, $KMgCl_3{\cdot}6H_2O$; Huff, 2016, 2019). It was further suggested that gravity-driven migration drove these high-density brines westward, where they were tectonically flushed into the overlying carbonate units (Huff, 2016, 2019). Although these hypotheses are compelling, to the best of our knowledge, there has been no direct evidence for the existence of Li-enriched late-stage evaporite minerals or hydrothermal transport.

Here we investigate the nearby Precambrian basement and its overlying siliciclastic and carbonate units, which Eccles and Berhane (2011) have suggested are the conduit for hydrothermal migration. We couple lithofacies analyses and Li-isotope geochemistry to examine three drillcores from west-central Alberta (Unique Well Identifier [UWI]: 14-02-077-22-W5, 09-16-076-21-W5, 10-27-080-08-W5). Sedimentological analysis reveals that these sediments were derived from a high relief crystalline structure and transported basinward along a system of laterally migrating fluvial channels into a shallow marine basin. Much like modern and near modern systems, we report that coarse-grained, superficially weathered lithologies show the lowest Li concentrations and highest δ^7Li values, whereas fine-grained lithologies characterized by the formation of secondary clay minerals host the highest Li concentrations and are enriched in ^6Li. Additionally, our results show a general dilution in Li concentration with distance from crystalline rocks of the Precambrian basement, as well as a lack of hydrothermal alteration in any of the five stratigraphic units analyzed in this study. Contrary to the prevailing assumption that Li in the WCSB was derived from a post-depositional influx of hydrothermal fluids, we show that Li was weathered from crystalline basement and emplaced syndepositional to the surrounding basin. Our findings are the first to characterize a Li source within the WCSB, revealing a clear correlation between the distribution of Li-rich weathered sediments and Li concentrations in formational waters. We propose a unifying hypothesis for Li cycling throughout the WCSB, integrating sedimentary processes and geochemical evolution.

Li isotope systematics are widely used in modern and near-modern settings to differentiate high-temperature hydrothermal processes from low-temperature weathering systems (i.e., Huh et al., 1998; Millot et al., 2010a; Araoka et al., 2014; Pogge von Strandmann et al., 2016; Tomascak et al., 2016; Godfrey and Álvarez-Amado, 2020). However, this is the first study to use Li isotopes to directly identify and trace Li from its source to its sink within a deep basin weathering regime. By integrating Li isotopes with sedimentological and hydrogeochemical data, we demonstrate a direct link between syndepositional processes and modern dissolved Li concentrations in groundwater. Although Li-rich groundwaters have been identified in deep sedimentary basins worldwide, including the WCSB, their sources and timing of emplacement remain poorly constrained. Without a more comprehensive understanding of the origins of Li in these basins, it is challenging to elucidate the mechanisms responsible for their enrichment or rationalize their spatial distributions. This study provides a novel methodology, leveraging Li isotopes to establish a framework for understanding the genesis of Li concentrations in deep-time contexts. This framework can be directly applied to analogous sedimentary basins globally, offering valuable insights to inform future Li exploration efforts.

Lithium Isotopes Background

Li has two stable isotopes, ^6Li and ^7Li, found in abundances of 7.52% and 92.48%, respectively (Jeppson et al., 1978). It is a fluid mobile element, and because of the large mass difference between isotopes (~15%), Li isotopes are prone to large fractionations during low-temperature water-rock interactions. Accordingly, Li isotopes have proven to be effective tracers of weathering processes (Huh et al., 1998; Tomascak, 2004; Millot et al., 2010a; Pogge von Strandmann et al., 2017; Kalderon-Asael et al., 2021). Both field and experimental studies show that during weathering, primary silicate minerals dissolve without significant fractionation of Li isotopes and that ^6Li is preferentially retained by secondary minerals (clays, zeolites, and oxyhydroxides). By contrast, ^7Li goes into solution, leaving the residual waters isotopically heavy (Huh et al., 1998, 2001; Pistiner and Hender-

son, 2003; Vigier et al., 2009; Wimpenny et al., 2010). Within the secondary silicate minerals, Li may be fixed into two isotopically distinct reservoirs (Pistiner and Henderson, 2003); structural incorporation strongly favors ^{6}Li. There is a weaker preference during sorption to exchangeable sites, leading to lower and potentially imperceptible fractionation factors (Pistiner and Henderson, 2003; Pogge von Strandmann et al., 2019). As a result of weathering processes, δ^{7}Li values across Earth's surface span more than 50‰, with Li sourced from continental crust (−10‰ to +10‰; mean = ∼+0.6‰) partitioning between solids (continental sediments: −7.0‰ to +22‰; mean = ∼−1.0‰), fresh water (rivers and lakes: +2.0‰ to +43‰; mean = ∼+23‰), seawater (+31‰), and marine sediments (−4.0‰ to +24‰; mean = ∼+4.4‰; see Chan et al., 1992; Huh et al., 1998; Pistiner and Henderson, 2003; Teng et al., 2004; Jeffcoate et al., 2004; Chan et al., 2006; Qiu et al., 2009; Tomascak et al., 2016).

Rivers are estimated to account for ∼50% of Li input into the oceans. Nonetheless, rivers have generally low Li concentrations (∼1.8 ppb), whereas terrestrial clay minerals have higher concentrations (∼5.0–300 ppm) suggesting a substantial proportion of Li derived from primary rocks is retained by secondary minerals on the continents (Huh et al., 1998; Tomascak et al., 2016; Pogge von Strandmann et al., 2020). The remainder originates from high-temperature hydrothermal fluids along mid-ocean ridges (Hathorne and James, 2006). Here, concentrations are considerably higher than in river systems, ranging from 0.1 ppm to 10 ppm, and δ^{7}Li values span a small range (+5.0‰ to +11.0‰; mean ∼+8.0‰) but are typically heavier than their source, mid-ocean ridge basalts (MORB, δ^{7}Li = ∼+4.0‰). The parameters controlling Li concentrations and isotopic fractionation in hydrothermal fluids is attributed to the temperature of the system, the primary minerals with which fluids interact, water/rock ratios, and the degree of water-rock interactions (Penniston-Dorland et al., 2017).

Although the stable (Ca, Mg, and Si) and radiogenic (Sr and Os) isotopes of other metals and metalloids are fractionated by weathering processes, Li isotopes exhibit several key advantages as a tracer (Pistiner and Henderson, 2003). Li concentrations in silicates (∼5.0–300 ppm; mean ∼60 ppm) are considerably higher than those in carbonates (0.02–21 ppm; mean ∼1.1 ppm), meaning Li isotopes, in essence, only track silicate weathering (Teng et al., 2004; Millot et al., 2010a; Romer et al., 2014; Tomascak et al., 2016; Pogge von Strandmann et al., 2020; Kalderon-Asael et al., 2021). No Li isotope fractionation has been observed by the growth of phytoplankton (Pogge von Strandmann et al., 2016), and although some fractionation of Li isotopes in plants has been reported by Li et al. (2020), other studies (Lemarchand et al., 2010; Clergue et al., 2015; Steinhoefel et al., 2021) report no fractionation. This suggests that Li may be one of a select group of elements that does not experience biologically mediated isotope fractionation (Pogge von Strandmann et al., 2020).

Geologic Setting of the Western Canada Sedimentary Basin

The WCSB is a northeast-tapering wedge of sedimentary rocks extending from southwestern Northwest Territories, across northeastern British Columbia and Alberta, and into southern Saskatchewan and Manitoba (Porter et al., 1982). Near its western extent, strata reach over 6 km in thickness and thin to 0 km in northeastern Alberta (Porter et al., 1982). The earliest sediments comprise a series of diachronous sandstones ranging in age from the Cambrian to Ordovician periods that were deposited following continental rifting in the late Precambrian eon (600–555 Ma) and the development of a cratonic platform along the western flank of North America (Porter et al., 1982; Bond and Kominz, 1984). The emerging passive margin was followed by a period of tectonic subsidence and sea level rise, which resulted in an extensive transgression of the North American Craton that led to deposition of the Sauk Sequence (Porter et al., 1982). Sea level continued rising through the Middle-Late Cambrian, overlaying transgressive cycles of deep marine siltstone and shale on the basal sandstones, and a subsequent lowering of sea level through the Ordovician led these deposits to grade into shallow water carbonates along the western margin of the basin (Aitken, 1971).

Following the decrease in sea level, an episode of erosion differentially removed Sauk Sequence deposits across the WCSB and left a widespread unconformity near the base of the Middle Ordovician (Aitken, 1971). In particular, the entire Sauk Sequence was removed along two northeast-trending bands across west-central Alberta and southwestern Northwest Territories, leaving the Precambrian basement exposed prior to the transgressive phase of the Middle Devonian period (Benvenuto and Price, 1979; Porter et al., 1982). In these regions, the complete removal of Sauk Sequence deposits is attributed to the uplift of a series of arches and ridges that extensively influenced the distribution of sediments throughout the Middle Devonian (Fig. 1; Cant, 1988; Porter et al., 1982). Three major structures are recognized: (1) the Tathlina High, located in northwestern Alberta and southwestern Northwest Territories; (2) the Peace River Arch (PRA), which lies along the British Columbia–Alberta border and extends into central Alberta; and (3) the West Alberta Ridge, which sits south of the PRA and parallels the passive margin in the approximate position where the front and main ranges of the Canadian Cordillera are today, potentially forming a continuation of the PRA landmass (Fig. 1; Moore, 1989; O'Connell et al., 1990).

The largest of these features is the PRA, which extends ∼700 km from northeastern British Columbia into central Alberta, reaching 800–1000 m above regional basement elevation to the west and 400–500 m above regional elevation at its eastern extent (Cant, 1988). It is ∼140 km wide and has an asymmetrical shape, dipping steeply to the north and gently to the south (Cant, 1988; O'Connell et al., 1990). Evidence suggests that uplift of the PRA was initiated by at least the Middle Cambrian and may have begun as early as the late Proterozoic. However, it is not believed to have grown into a prominent feature until sometime thereafter and did not achieve peak relief until the Early-Middle Devonian (Cant, 1988; O'Connell et al., 1990; McMechan, 1990). The Tathlina High is a smaller cratonic arch that is believed to have initiated in the Middle Cambrian (Porter et al., 1982). It is not known when the West Alberta Ridge developed; nonetheless, by the Middle Devonian these structures were high-standing topographic features that restricted seawater circulation into the basin and enclosed topographic depressions to the north and south of the PRA. This facilitated sediment shedding during renewed cycles of transgression and regression until their burial in the Late Devonian (Porter et al., 1982; Trotter, 1989).

The origins of the PRA remain under debate. Theories for the upward movement of Precambrian rock include: doming due to a mantle hotspot (Burwash and Krupička, 1970; Stelck, 1975; Stelck et al., 1978); a failed Paleozoic rift system (Cant, 1988); transform faulting along a mid-ocean ridge (O'Connell et al., 1990; McMechan, 1990); and flexural uplift of the basement (Beaumont et al., 1993). Regardless of the mechanism, the PRA remained tectonically active throughout the entirety of its history, with early uplift and extension resulting in numerous high-relief horsts and grabens from the Cambrian to the Middle Devonian. This was followed by post-burial subsidence and syn-sediment accumulation in the Mississippian period, renewed extension in the Pennsylvanian period, stability through the Permian period, and an overall collapse into the Mesozoic era (Sikabonyi and Rodgers, 1959; Cant, 1988; O'Connell et al., 1990;

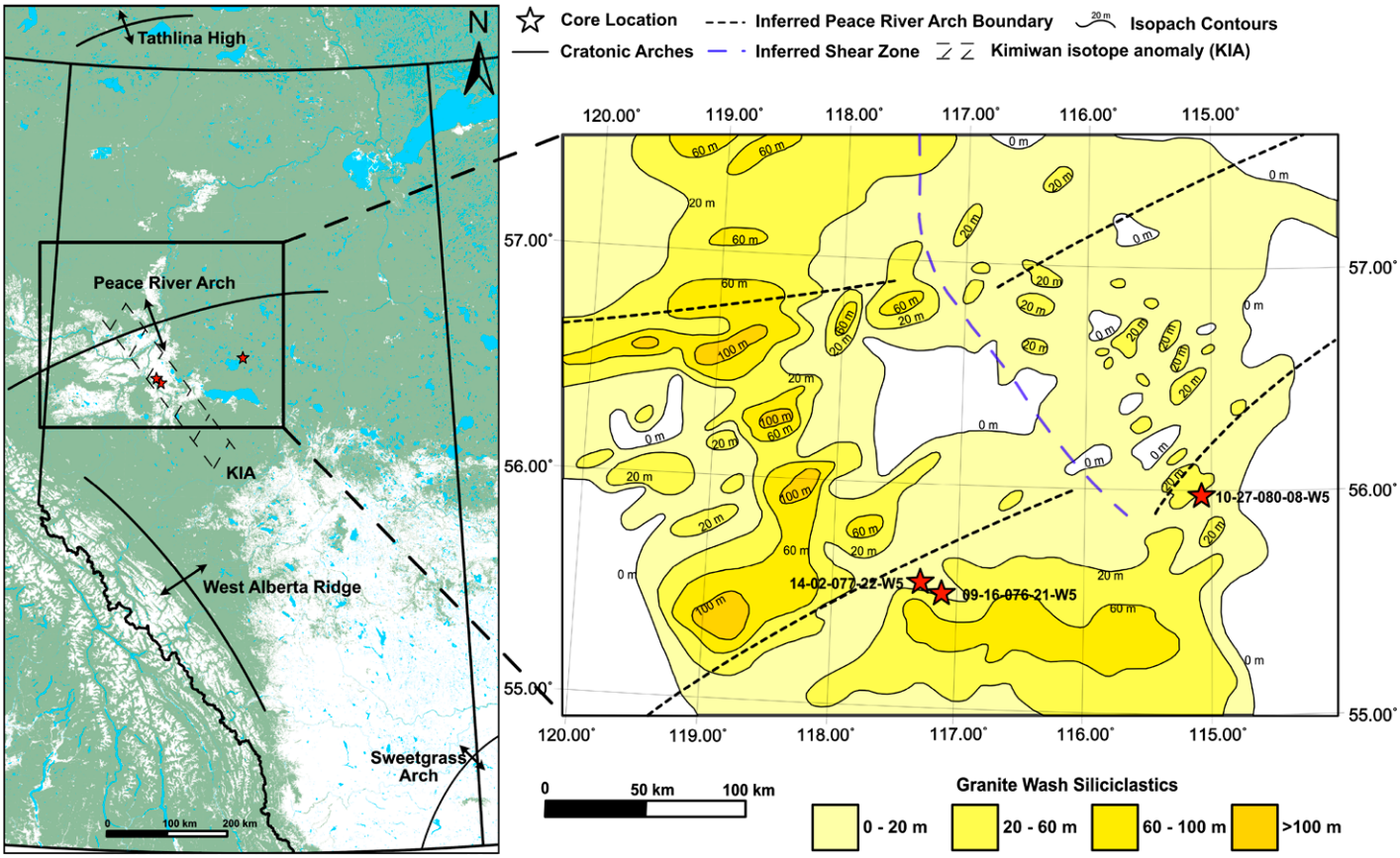

Figure 1. (Left) Location of cratonic arches and ridges that influenced deposition throughout the Devonian in the Western Canada Sedimentary Basin (modified from Cant, 1988; O'Connell et al., 1990). (Right) Isopach of the Granite Wash (20 m contours) along the extent of the Peace River Arch (PRA), and the location of core used in this study (red stars; modified from Trotter and Hein, 1988). The approximate edges of the PRA are represented by narrow dashed lines.

Balshaw, 2010). By the Late Cretaceous, partial reactivation of the basement raised the PRA to a subtle high until its reburial near the end Cretaceous (Donaldson et al., 1999).

In addition to the normal faulting associated with uplift of the PRA, a more ancient, localized zone of extensional faulting has been recognized within Precambrian basement rocks named the Kimiwan isotope anomaly (Burwash et al., 2000). Here, high grade minerals show retrograde alteration to chlorite and epidote and feature anomalously low $\delta^{18}O$ values, which are interpreted to result from extensional faulting and fluid-rock interactions with meteoric water at ca. 1800 Ma (Burwash et al., 2000). The Kimiwan isotope anomaly extends roughly perpendicular to the trend of the PRA covering an area ~250 × 50 km (Fig. 1; Burwash et al., 2000). Although the Kimiwan isotope anomaly is much older than more regional Tathlina High, PRA, and West Alberta Ridge, periodic reactivation of these basement faults are credited with the development of faults in the overlying Phanerozoic strata (Burwash et al., 2000).

Local Geology of the Peace River Arch and Study Area

Following erosion of the Sauk Sequence, the earliest deposits to blanket the PRA comprise diachronous siliciclastics of the Granite Wash, which are sediments derived from, and unconformably overlying, the granitic and gneissic Precambrian basement rocks that make up the PRA (Figs. 1 and 2; Cant, 1988; Trotter and Hein, 1988). Granite Wash sediments can be found within the shallow marine environments flanking the arch, along the limbs of the uplift, and within fault-bounded grabens and other paleotopographic lows on the crest, where they reach over 100 m in thickness (Dec et al., 1996). To the north and south of the PRA, the Granite Wash forms widespread sandstone units deposited in fluvial, fan-delta, and shallow marine complexes, which interfinger with onlapping transgressive deposits of the Middle-Late Devonian (Trotter and Hein, 1988; O'Connell et al., 1990). Toward the lower relief, eastern extent of the PRA, the Granite Wash forms narrow sand bodies deposited in fluvial and possibly estuarine environments (Trotter and Hein, 1988). The age of the Granite Wash is unknown, except where they interfinger with Middle-Late Devonian strata (O'Connell et al., 1990).

As previously mentioned, the PRA, West Alberta Ridge, and Tathlina High were prominent features by the Middle Devonian, and seawater circulation into the basin was severely restricted (Hauck and Grobe, 2020; Porter et al., 1982). The result was an accumulation of evaporites, carbonates, and clastics of the Elk Point Group, which were the first sediments to onlap the PRA and interfinger with stratigraphically equivalent, backstepping Granite Wash sediments (Fig. 3A; Hauck and Grobe, 2020; O'Connell et al., 1990). Carbonate and evaporite successions in north-central Alberta make up the Muskeg Formation (Hauck and Grobe, 2020). Southeastward, the WCSB became increasingly evaporitic and lateral equivalents to the Muskeg Formation were primarily composed of halite and sylvite (Hauck and Grobe, 2020). Transgression through the Middle Devonian was punctu-

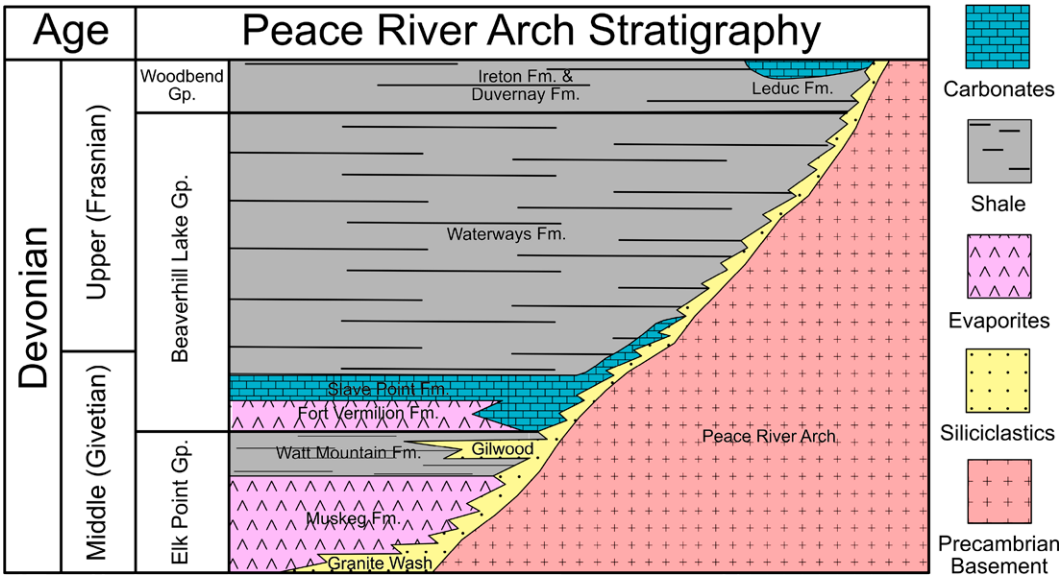

Figure 2. Middle to Late Devonian stratigraphy around the Peace River Arch (PRA) following complete erosion of the Sauk Sequence. Diachronous siliciclastics of the Granite Wash drape across the Precambrian Basement. Restricted seawater exchange with the open ocean led to the deposition of extensive evaporites of the Muskeg Formation, following which sea level rise capped the Elk Point Group with marginal-marine brackish and lacustrine shales of the Watt Mountain Formation (Hauck and Grobe, 2020). Several brief, punctuated events of regression led to the progradation of arch-derived siliciclastics into the basin, the most extensive of which is the Gilwood Member (Williams, 1997). Following deposition of the Gilwood Member, a short period of sea level standstill or slight regression led to the deposition of evaporitic sequences of the Fort Vermilion Formation, and the eventual resumption of sea level rise led to the flooding of these deposits and development of the Slave Point Formation carbonate platform around the PRA (Jansa and Fischbuch, 1974; Hauck, 2014).

ated by several regressive events in which arch-derived siliciclastics prograded into the basin (e.g., Balshaw, 2010). The Gilwood Member is the most prominent incursion, interpreted as a fluvio-deltaic transitional sequence that developed along an extensive coastal plain swelling from the arch (Fig. 3B; Williams, 1997; Shawa, 1969; Jansa and Fischbuch, 1974).

The PRA remained an emergent, topographic high following deposition of the Elk Point Group, when a brief period of sea level standstill or slight regression led to the development of evaporitic sequences conformably overlying shales and terrigenous clastics of the Watt Mountain Formation and fluvio-deltaic deposits of the Gilwood Member (Fig. 3B; Hauck, 2014; Jansa and Fischbuch, 1974). These evaporites comprise the Fort Vermilion Formation and consist of massive to nodular anhydrites interbedded with dolomitic muds and laminated anhydrite (Hauck, 2014). They are characterized as supratidal, intertidal, and lagoonal deposits that pinch out toward the PRA and extend up to 80 km into the basin, thickening up to ~25 m (Fig. 3C; Keith, 1990; Jansa and Fischbuch, 1974).

Sea level continued rising with the overall transgressive phase of the Middle-Late Devonian, and evaporites of the Fort Vermilion Formation were conformably overlain by carbonates of the Slave Point Formation (Fig. 3D; Hauck, 2014). Slave Point strata are characterized by a fossiliferous lime mudstone that reaches ~12 m thickness away from the PRA and extends beyond the underlying Fort Vermilion evaporites toward the arch, onlapping Granite Wash sediments (Keith, 1990; O'Connell et al., 1990). Transgression of the WCSB continued for the remainder of the Middle-Late Devonian, leading to an accumulation of open marine calcareous shales and nodular limestones of the Waterways Formation (Jansa and Fischbuch, 1974).

In this study, we examine three cores from north-central Alberta (UWI locations: 09-16-076-21-W5, 14-02-077-22-W5, 10-27-080-08-W5) for their Li content and Li isotopic values. These cores are located along the southern flank of the PRA, reaching from the Precambrian basement upward through the overlying Granite Wash, Muskeg Formation, Watt Mountain Formation, Gilwood Member, and Slave Point Formation (Fig. 2). The hypothesis of hydrothermal emplacement suggests sandstones of the Granite Wash and Gilwood Member to be the conduit for fluids mobilized from the basement, and the overlying Muskeg Formation, Watt Mountain Formation, and Slave Point Formation have previously been recognized to host Li-rich brines (Hitchon et al., 1993; Eccles and Berhane, 2011). Two of the cores (UWI locations: 14-02-077-22-W5, 09-16-076-21-W5) examined in this study are located within the Kimiwan isotope anomaly, which is the zone hypothesized to be responsible for hydrothermal upwelling, while the third core (UWI location: 10-27-080-8-W5) is located away from the Kimiwan isotope anomaly, toward the eastern flank of the PRA (Fig. 1).

METHODS

A detailed description of the methods used in this study is outlined in Section 1 of the Supplemental Material.[1] Briefly, they include core logging and sample collection, followed by powder X-ray diffraction, bulk leaching of the carbonate material, and bulk digestion of the silicate material. All samples were measured for their bulk Li content with a Thermo Scientific Element XR ICP-MS (inductively coupled plasma–mass spectrometry), and Li isotopic measurements were conducted using a Thermo Finnigan Neptune Plus multicollector (MC)-ICP-MS. Lithium concentration and isotope work followed the methods detailed in Kalderon-Asael et al. (2021). Error on the concentration and isotopic measurements, based on repeat analysis of SBC-1, BHVO-2, L-SVEC-1, and Atlantic seawater in the same batches as our samples was better than 6.6% and better than 0.07‰. Jeffcoate et al. (2004) previously characterized the δ^7Li value of modern seawater for use as a reference material and measured 31.1‰ (±0.20‰). In this study, our repeat measurements of Atlantic seawater returned values of 31.05‰ (±0.16‰).

[1]Supplemental Material. Methodology, lithofacies, depositional setting, and Supplemental Plates S1–S3. Please visit https://doi.org/10.1130/GSAB.S.29189762 to access the supplemental material; contact editing@geosociety.org with any questions.

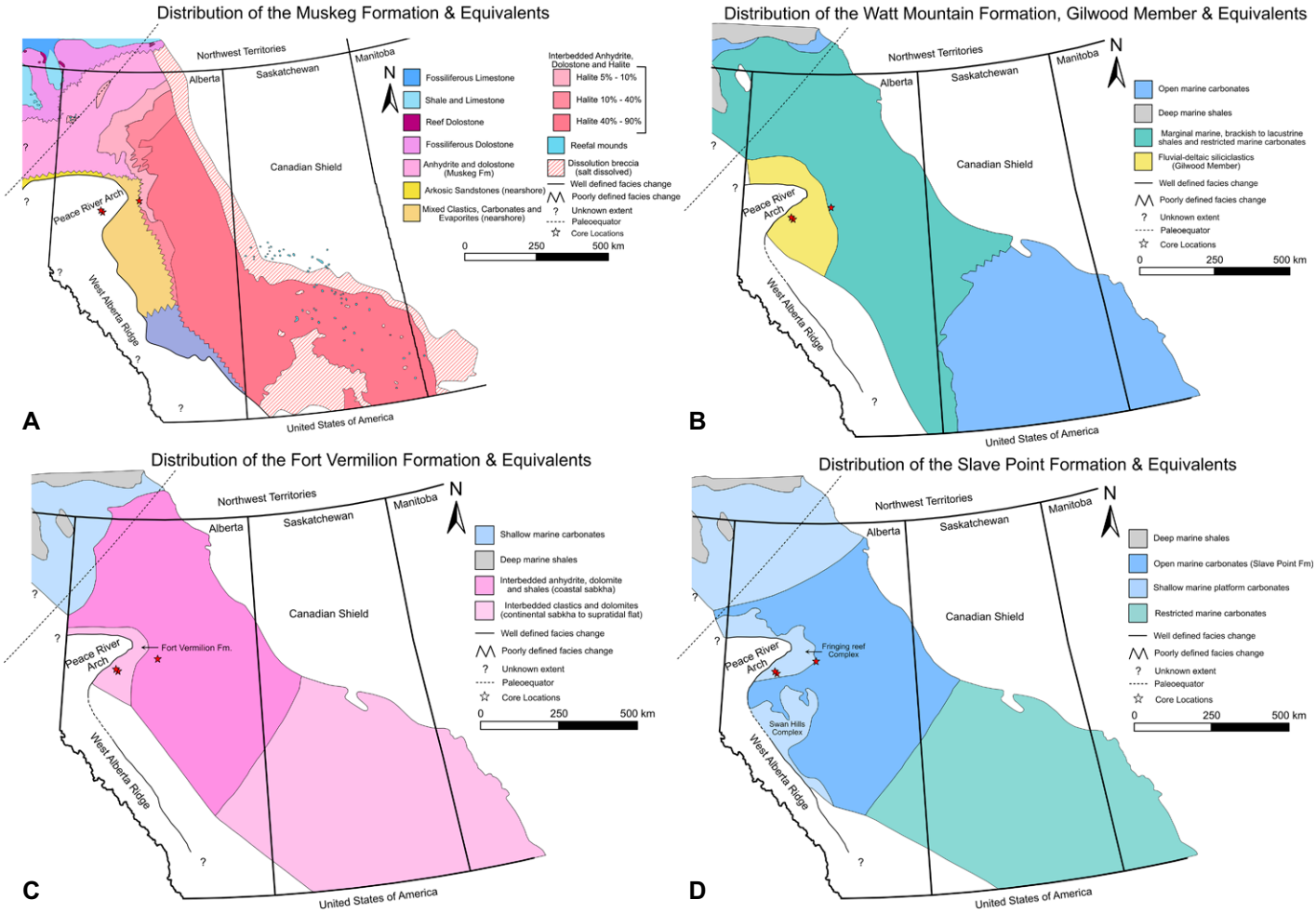

Figure 3. Distribution of Western Canada Sedimentary Basin (WCSB) sediments throughout the Middle Devonian (Middle-Late Givetian). (A) Distribution of the Muskeg Formation and its equivalents across the WCSB (modified from Drees et al., 1994). Restricted seawater circulation coupled with a near equatorial location led to the deposition of extensive, thick evaporites across the WCSB. The Muskeg Formation is the first sediments to onlap the Peace River Arch (PRA) and interfinger with stratigraphically equivalent backstepping Granite Wash sediments (Hauck and Grobe, 2020). It is dominated by anhydrite and dolomite that become more evaporative in its equivalent units toward the south-southeast into central Alberta and southern Saskatchewan, where the sediments comprise up to 90% halite (modified from Drees et al., 1994). (B) Transgression into the basin deposited marginal-marine, brackish water and lacustrine shales and carbonates across the Alberta basin and into south-central Saskatchewan (modified from Drees et al., 1994). The Watt Mountain Formation is characterized by several punctuated periods of regression in which arch-derived clastics prograded into the basin. The Gilwood Member is the most prominent incursion, interpreted as a fluvial-deltaic transitional sequence that developed along an extensive coastal plain swelling from the arch (Williams, 1997, Shawa, 1969). (C) Following deposition of the Watt Mountain Formation and Gilwood Member, sea level remained at a standstill or slightly regressed, leading to the development of a continental to supratidal sabkha around the PRA and coastal sabkha in the surrounding area (modified from Drees et al., 1994). (D) The overall transgressive phase of the Middle-Late Devonian resumed, flooding the evaporitic deposits into shallow and open marine environments (Hauck, 2014). A carbonate platform developed along the flanks of the PRA as well as the nearby West Alberta Ridge (modified from Drees et al., 1994). Red stars indicate the locations of cores used for this study.

Geological Lithofacies and Depositional Setting

Table 1 provides a summary of each facies including the lithologic characteristics, mineralogy, and whether or not trace fossils are present. It outlines lithofacies associations, the nature of their contacts, and interpreted depositional environment. Section 2 of the Supplemental Material provides full descriptions of each lithofacies and interpretations of their depositional setting. Plates exhibiting the core expression of each facies are also given in the Supplemental Material (Supplemental Plates S1–S3).

Li Isotopic Contents and Concentrations of Lithofacies

Lithium was identified in all 56 samples, covering a broad extent of bulk composition and isotopic values, with concentrations ranging from 0.4 ppm to 167.3 ppm and δ^7Li values ranging

TABLE 1. SUMMARY OF THE LITHOFACIES IDENTIFIED IN THE CORES, THEIR ASSOCIATIONS WITH OTHER LITHOFACIES, AND INTERPRETATIONS OF THEIR DEPOSITIONAL ENVIRONMENTS

Facies	Lithologic characteristics	Trace fossils	XRD mineralogy	Facies associations	Interpretation
Facies 1—Deformed to recrystallized alkali feldspar granites and granitic pegmatites	Recrystallized and deformed granites and granitic pegmatites. Alkali feldspars constitute a major component of the facies with generally large crystals reaching up to 4 cm in length. Recrystallized rocks are heavily fractured.	N/A	Microcline, epidote, muscovite (Li-bearing), siderophyllite (Li-bearing), clinochlore, chalcopyrite	Overlain by Facies 2	Precambrian basement
Facies 2—Matrix supported breccia	Structureless to weakly stratified matrix supported breccia. Matrix ranges from clay to very coarse sand and hosts granule to pebble sized angular clasts. Clasts are composed of granitic rocks and primary igneous minerals.	N/A	N/A	Sharply overlies Facies 1	Regolith
Facies 3—Massive to normal graded and cross stratified pebbly sandstone	Cm-dm scale massive to normal graded and high angle cross stratified pebbly sandstones. Crude planar and convolute bedding may also be found. Beds are sharp based and filled with granule to pebble sized clasts of feldspar, quartz, and mudstone. Sandstone is composed of subangular to subrounded medium–very coarse arkosic sands.	N/A	Quartz, microcline, halite	Occurs interbedded with Facies 2, 4, 5, 8, and 9	Bar and lag deposits of braided fluvial channels
Facies 4—Red to green mottled silty sandstone, shale, and mudstone	Interbedded reddish-purple to green-grey mottled silty sandstone, shale, and mudstone. Silty sandstones dominate the lower part of the facies and progressively become finer grained into blocky mudstones. Sharp based beds that may incorporate clasts from the underlying unit. Slickenside and carbonized rootlets occur throughout.	N/A	Quartz, microcline, orthoclase, muscovite, kaolinite	Interbedded with Facies 3, 6, and 8	Pedogenically altered overbank floodplain deposits (paleosols)
Facies 5—Massive dolomitic mudstone	Massive dolomitic mudstone containing rare, mm-scale microbial laminae. Planar laminae can be found; however, they tend to be weakly defined. Rare fracturing is infilled with secondary anhydrite.	N/A	Dolomite, quartz, muscovite	Interbedded with Facies 3 and 4	Restricted nearshore lagoon
Facies 6—Planar laminated convolute dolomite, anhydrite, and halite	Planar to convolute laminated dolomite, anhydrite, and halite. Anhydrite and dolomite laminae range from 2 mm to 6 mm in thickness. Dolomitic muds dominate the lower portion of the facies and the relative proportion of anhydrite and halite increase up section.	N/A	N/A	Gradational contact with Facies 5	Deep lagoon laminates
Facies 7—Microbially laminated calcareous mudstone	Planar bedded to microbially laminated calcareous mudstone. Microbial laminae occur throughout; however, their frequency increases up section where they reach a maximum thickness of ~3 mm. Brecciated anhydrite clasts may be found floating in calcareous muds.	N/A	N/A	Gradational contact with Facies 6	Lagoon edge
Facies 8—Heterolithic very fine to medium grained sandstone	Planar to low angle cross stratified fine to medium grained arkosic sandstones interbedded with heterolithic fine grained sandstone. Sandstones are well sorted and made up of subangular to rounded grains. The proportion of mud tends to increase up section with the development of flaser and wavy bedding.	N/A	Quartz, orthoclase, microcline, muscovite, kaolinite, pyrite, dolomite	Facies 3 grades into Facies 8	Distal bar deposits of the delta front
Facies 9—Bioturbated silty sandstone	Planar laminated to pervasively burrowed silty sandstone. Burrowed beds are recurring and sporadically distributed throughout the facies. Burrows tend to increase in both size and diversity up section.	*Chondrites, Planolites, Arenicolites, Diplocraterion* and *Cylindrichnus* BI = 2–6	Quartz, orthoclase, microcline, muscovite, kaolinite, pyrite, dolomite	Occurs interbedded with Facies 8 and may be sharply overlain by Facies 3	Proximal prodelta
Facies 10—Nodular wackestone interbedded with calcareous mudstone	Nodular wackestone interbedded with planar laminated to massive calcareous mudstone. Secondary calcareous nodules dominate a large portion of this facies, disrupting nearly all original bedding. Brachiopods and crinoids are common, but tend to be disarticulated, fragmented, and concentrated in sharp based, cm-dm scale beds.	N/A	Calcite, quartz, dolomite, pyrite, muscovite	Gradational contact with Facies 10	Carbonate platform above storm wave base
Facies 11—Blocky brown/green mudstone	Planar laminated to massive block brown/green mudstone. This facies is sharp based and angular mudstone clasts occur sporadically throughout.	*Chondrites.* BI = 1	Quartz, dolomite, nontronite, muscovite, smectite, Montmorillonite, jasmundite, clintonite, vermiculite	Sharply overlies Facies 8	Shallow brackish–freshwater coastal plain

Note: Together these span a weathering profile from crystalline basement of the Peace River Arch through fluvial channels draining the cratonic uplift to several Middle Devonian transgressive-regressive events, which led to various onlapping lithologies. In total, these facies represent six stratigraphic units ranging from (1) Precambrian basement, (2) fluvial siliciclastics of the Granite Wash, (3) lagoonal evaporites and carbonates of the Muskeg Formation, (4) fluvial-deltaic siliciclastics of Gilwood Member, (5) brackish-freshwater mudstones of the Watt Mountain Formation, and (6) platform carbonates of the Slave Point Formation. BI—Bioturbation Index.

TABLE 2. LITHIUM ISOTOPE AND BULK CONCENTRATIONS OF SELECTED ROCK SAMPLES FROM THE THREE CORES ANALYZED IN THIS STUDY

Sample ID	δ^7Li (‰)	Standard error (‰)	Li concentration (ppm)
14-02-077-22-W5			
D-001	5.9	0.04	109.8
D-002	3.0	0.04	103.4
D-003	8.5	0.03	94.0
D-004	18.8	0.04	2.1
D-005	19.7	0.03	4.5
D-006	7.6	0.03	167.3
D-007	7.8	0.03	85.2
D-008	7.1	0.04	152.4
D-009	7.9	0.04	66.2
D-010	7.6	0.03	147.1
D-011	7.2	0.03	77.8
D-012	17.8	0.04	4.6
D-013	8.0	0.04	137.0
D-014	7.5	0.03	110.7
D-015	7.3	0.03	80.5
D-016	7.1	0.03	78.6
D-017	7.0	0.05	48.9
D-018	23.3	0.04	1.6
D-019	2.6	1.77	7.6
D-020	9.3	0.03	86.6
09-16-076-21-W5			
G-001	7.7	0.02	48.6
G-002	11.9	0.04	4.0
G-003	7.2	0.04	81.6
G-003 dup	7.1	0.05	80.3
G-004	6.6	0.03	109.4
G-005	16.5	0.03	3.4
G-006	7.9	0.03	34.2
G-007	9.5	0.03	1.4
G-008	14.3	0.04	2.7
G-009	14.0	0.04	2.8
G-010	10.4	0.03	0.4
G-011	16.7	0.07	1.4
10-27-080-08-W5			
N-001	6.1	0.03	22.5
N-002	3.4	0.04	21.7
N-003	6.4	0.03	29.0
N-004	16.7	0.04	17.5
N-005	1.5	0.04	66.4
N-006	16.0	0.03	15.0
N-007	7.3	0.03	28.2
N-008	6.2	0.03	36.4
N-009	10.6	0.04	27.5
N-010	22.0	0.05	0.4
N-011	6.7	0.03	1.4
N-012	8.1	0.03	127.6
N-013	6.8	0.03	166.4
N-014	23.5	0.04	16.5
N-015	3.7	0.04	46.0
N-016	12.8	0.03	16.0
N-017	6.1	0.04	67.5
N-018	5.7	0.04	52.4
N-019	7.3	0.04	96.5
N-020	7.2	0.03	43.7
N-021	19.5	0.03	14.6
N-022	6.7	0.03	70.0
N-023	6.7	0.04	5.6
N-024	16.4	0.04	5.6
N-025	19.6	0.03	3.1

Geostandards	Average δ^7Li (‰)	Standard deviation	Li concentration (ppm)	Recovery (%)
L-SVEC-1 (n = 4)	−0.05	0.16	-	-
Atlantic seawater (n = 4)	31.05	0.16	-	-
BHVO-2 (n = 5)	-	-	4.43	98.44%
SBC-1 (n = 6)	-	-	153.89	94.41%

Note: Isotopic measurements were obtained via multicollector–inductively coupled plasma–mass spectrometry (MC-ICP-MS) and Li concentrations were determined by ICP-MS. The normalized isotopic notation of Li was calculated and reported relative to the L-SVEC-1 lithium carbonate standard, and Atlantic seawater was measured for comparison. Georeference standards BHVO-2 and SBC-1 were digested and analyzed along with each batch of rock samples to determine bulk Li recovery.

from 1.5‰ to 23.5‰ (Table 2). Figure 4 outlines the log of each core highlighting sample locations and the distribution of lithologic characteristics, facies, isotopic composition, and Li content. Figure 5 shows a scatter plot of all Li isotopic measurements and concentrations by facies. A scatter plot of Li isotopic compositions and concentrations separated by core is found in the Supplemental Material. Samples from the crystalline basement of Facies 1 all measured within a narrow δ^7Li range (3.0‰–6.4‰), regardless of whether they were deformed or altered. However, the altered and recrystallized basement samples from UWI: 14-02-077-22W5 (103.4–109.8 ppm) notably contain ~4 times more Li than those that are not altered from UWI: 10-27-080-08-W5 (21.7–29.0 ppm). Facies 2 regolith was only sampled from the altered basement core (UWI: 14-02-077-22-W5) and showed a slightly more positive δ^7Li value (8.5‰) and lower concentration (94.0 ppm) compared with the directly underlying basement. The sharp based, pebbly channel sandstones of Facies 3 mark the base of the Granite Wash and an abrupt shift in Li content and isotopic composition. Facies 3 sediments are markedly more enriched in ^{7}Li (6.2‰–23.5‰) and have lower Li concentrations (2.1–36.5 ppm). It is worth noting that sample N-008 (6.2‰; 36.5 ppm) is an outlier in Facies 3 with respect to both Li isotopic content and Li concentration, where the remaining samples average 17.2‰ and 12.2 ppm. Facies 4 also makes up the Granite Wash, where floodplain paleosols developed along the banks of fluvial channels draining the PRA. They record the highest Li concentrations of all samples (28.2–167.3 ppm) and show a narrow range of δ^7Li values (1.5‰–8.1‰).

Facies 5 characterizes the base of the Muskeg Formation and Facies 6 and 7 record a transition into marginal-marine sediments onlapping the PRA. A single sample from the restricted lagoon dolomitic mudstones of Facies 5 revealed limited Li content (0.4 ppm) and high enrichment in ^{7}Li (δ^7Li = 22.0‰). A single sample from deeper lagoon laminated evaporites of Facies 6 also displayed a low Li concentration (1.4 ppm). However, they are isotopically lighter than their shallow water counterpart (6.7‰). Microbially laminated calcareous mudstones of Facies 7 were not sampled for analysis in this study, although it is worth noting that this facies only appears once in all three cores and accounts for only ~70 cm of the >60 total m of material that were assessed in this study.

Facies 8 and 9 comprise the Gilwood Member and represent fluvial-deltaic siliciclastics prograding into the basin during the subsequent fall in relative sea level. Distal bar sandstones of Facies 8 display a considerable range of both Li concentrations (1.6–80.5 ppm) and δ^7Li values (2.6‰–23.3‰). Facies 9, consisting of bioturbated silty sandstones of the prodelta, similarly display a broad extent of concentrations (1.4–86.6 ppm), but their Li isotopic values fall within a distinctly narrow range (6.8‰–9.5‰). A modest rise in relative sea level flooded the Gilwood Member and led to deposition of Facies 11 comprising brackish and freshwater mudstones of the Watt Mountain Formation. Analysis of Facies 11 indicated low Li content (3.1–5.6 ppm) and enrichment in ^{7}Li (16.4‰–19.6‰). Continued sea level rise led to

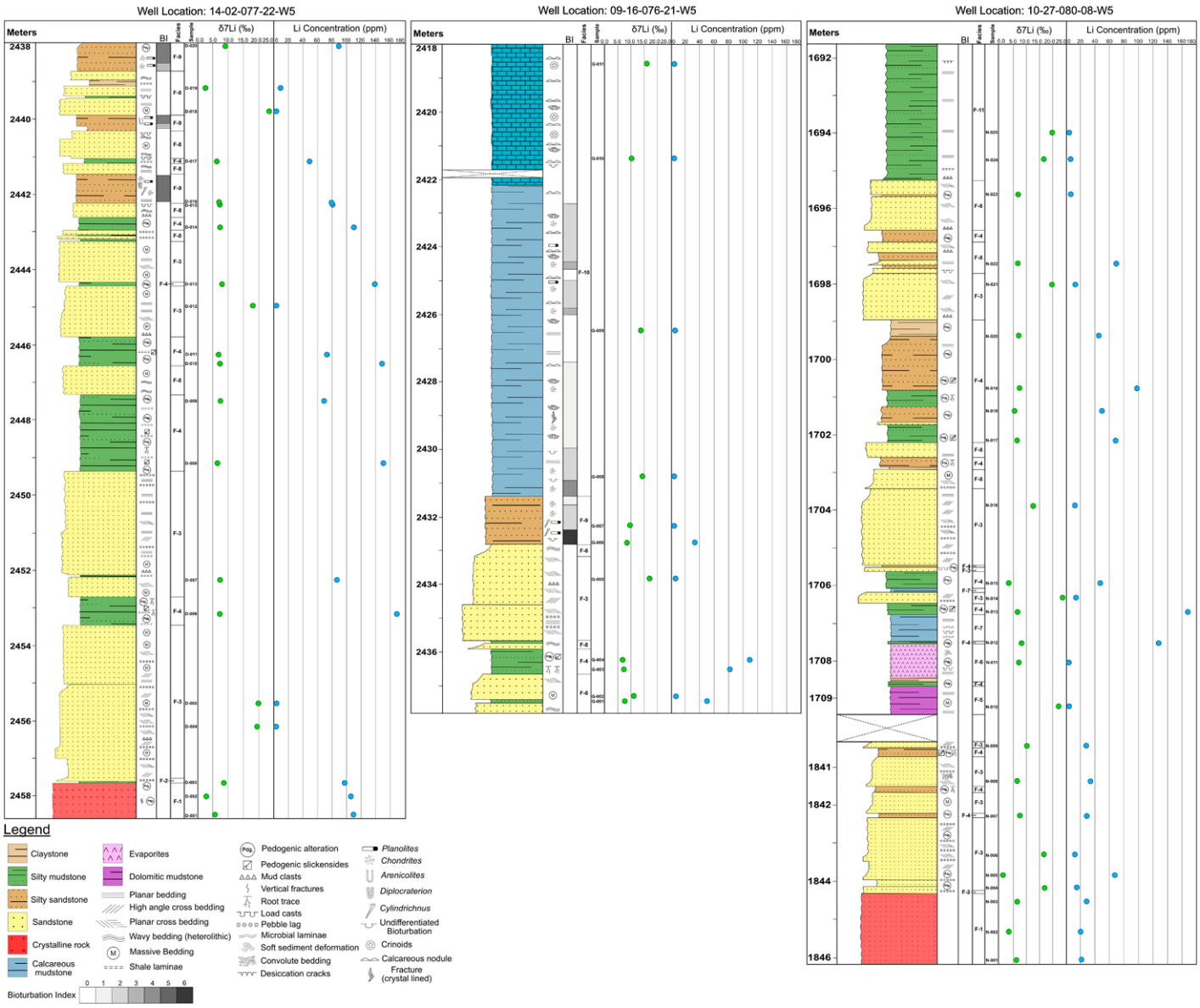

Figure 4. Stratigraphic logs outlining the lithofacies and Li concentration and isotopic values identified in three cores from UWI: (top) 10-27-080-08-W5; (middle) 14-02-077-22-W5; and (bottom) 9-16-076-21-W5. Li isotopes are reported as δ^7Li and concentrations are reported in parts-per-million (ppm) and outlined in Table 2. Missing core is denoted by a dashed "X" and all legend information are provided in each log. A summary of all facies is provided in Table 1, and core expressions of each facies are outlined in Supplemental Plates S1–S3 (see text footnote 1). A summary of δ^7Li values and Li concentrations is provided in Table 1. BI—Bioturbation Index.

the development of shallow marine onlap of the PRA and deposition of Facies 10 carbonates of the Slave Point Formation. Platform carbonates of Facies 10 returned the lowest Li concentrations of all samples (0.4–2.8 ppm) and tend to show moderate to high δ^7Li values (10.4‰–16.8‰).

Source of Li and Controls on Its Distribution

Basement Weathering

Previous investigations into Li sources to the Alberta Basin were limited to interpretations based on H, O, and Sr isotopic variations and trace metal geochemistry of the basinal brines (Eccles and Berhane, 2011; Huff, 2016, 2019). An analysis of the highly concentrated brines found in west-central Alberta explored various basement features as potential sources of Li. However, it ultimately proposed the source as a post-depositional influx of hydrothermal fluids expelled upward through the Kimiwan isotope anomaly. These fluids were proposed to have migrated along permeable siliciclastics of the Granite Wash and Gilwood members before moving into the overlying carbonate strata (Eccles and Berhane, 2011; Huff, 2019).

Of relevance to hydrothermal fluids, the fractionation of Li isotopes is dependent on temperature. Several studies have noted that as the temperature of the fluid increases during water-rock interactions, the degree of Li isotope fractionation decreases ($\delta^7Li_{solid} - \delta^7Li_{solution} = \Delta^7Li_{solid\text{-}solution}$) (Penniston-Dorland et al., 2017). Experimental and field examinations of hydrothermal fluids interacting with basalts from mid-ocean ridges show $\Delta^7Li_{solution\text{-}solid}$ values of 4.0‰ at 350 °C, 6.7‰ at 250 °C, 9.0‰ at 160 °C, and

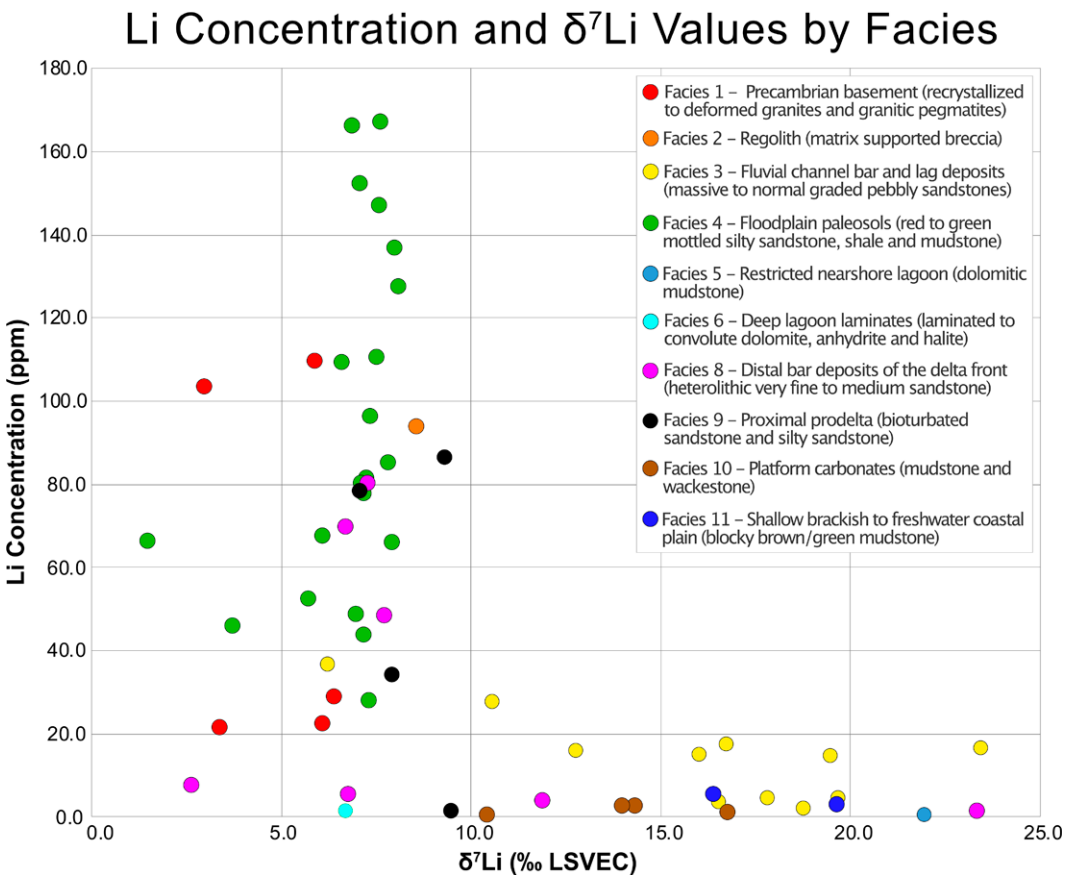

Figure 5. Scatter plot of Li isotopic compositions and bulk concentrations of samples grouped by facies.

19.0‰ at 25 °C (Chan et al., 1993, 1994; Millot et al., 2010b). Similarly, Pogge von Strandmann et al. (2016) measured δ^7Li values of relatively cold (3.0–7.0 °C) continental groundwaters and compared them with hydrothermal springs (200–300 °C), which have cooled during transport (17–44 °C). They reported that isotopic values remained low (δ^7Li: 4.9‰–10‰) even in the cooled hydrothermal waters and were similar to δ^7Li values for waters >350 °C, whereas δ^7Li values for the cold groundwaters were considerably larger in magnitude, ranging from 15.3‰ to 27‰. Pogge von Strandmann et al. (2016) attributed these variations to the production of secondary clay minerals at varying temperatures, as has been observed during chemical weathering of rocks. In high temperature geothermal waters, secondary mineral formation is inhibited, leading to lesser fractionation of Li isotopes, whereas low temperature systems promote formation of authigenic clay minerals, which preferentially incorporate ^{6}Li, during water-rock interaction (Pogge von Strandmann et al., 2016; Millot et al., 2010b).

With respect to Li concentrations, Chan et al. (1994) found hydrothermally altered sediments from Guaymas Basin in the Gulf of California to be similarly depleted in Li (11.5–20.8 ppm) compared with the overlying unaltered sediments (37.5–41.0 ppm). Their experimental results further demonstrated that elevated temperatures reduce the capacity of secondary minerals to retain Li, leading to significant leaching of Li from host sediments. In all cases, increasing temperature decreases the magnitude of Li isotope fractionation and increases the mobility of Li in fluids, leaving the host rocks depleted and solutions enriched in Li concentrations (Chan et al., 1994; Araoka et al., 2014).

Despite two of the three cores being located within the Kimiwan isotope anomaly, we observed no visual, mineralogical, or geochemical evidence of hydrothermal alteration or overprinting throughout any of the basal siliciclastics or onlapping stratigraphic units. The ranges of Li concentrations and Li isotopic values vary by nearly 167 ppm and 22‰, respectively, and, as is illustrated in Figure 5, these distributions are facies-dependent and display a similar profile across all three cores, regardless of their location. As expected from previous reports of the Li isotopic content of continental crust ($\delta^7\text{Li} = -10‰ \pm 10‰$; mean $\sim$0.6‰ $\pm$ 0.6‰), the δ^7Li values of crystalline basement were found to lie within a relatively narrow range of 3.0‰–6.4‰ across both drill cores from the PRA. However, within the deformed but unaltered basement, Li concentrations range from 21.7 ppm to 29.0 ppm but reach 103.4–109.8 ppm in the recrystallized basement, indicating that the recrystallized rocks host $\sim$4× more Li (Tomascak et al., 2016). Lithium is an incompatible element in magmatic systems, leading to its enrichment in increasingly felsic melts (Huh et al., 1998). As such, Li concentration increases from the primitive mantle (1.4 $\pm$ 0.1 ppm), through mid-ocean ridge basalts (5.5 $\pm$ 3.8 ppm), and into bulk continental crust ($\sim$18 ppm) and upper continental crust (35 $\pm$ 11 ppm; see Tomascak et al., 2016; Marschall et al., 2017; Teng et al., 2004).

Given that a significant proportion of the undeformed basement consists of biotite and large potassium feldspar crystals, it appears unlikely that these primary igneous minerals host any more Li than average continental crust. Instead, in early studies on the basement of the WCSB, Burwash and Krupička (1969, 1970) identified a zone of deformation and potassium metasomatism named the Athabasca Mobile Zone trending northeast through the PRA and into a large portion of west-central Alberta. They found that metaso-

matic recrystallization significantly increased the proportion of silicate and alteration minerals and suggested that the resulting decrease in average rock density was responsible for upward movement of the PRA (Burwash and Krupička, 1970). The K-metasomatized rocks notably showed the largest changes in potassium feldspar, muscovite, and epidote content, increasing on average by 73%, 383%, and 484%, respectively, compared to nearby unaltered basement (Burwash and Krupička, 1970). Considering the highly altered basement from UWI: 14-02-077-22-W5 contains nearly 4× more Li than the unaltered basement and 3× the Li of average continental crust, it seems likely that Li was mobilized into the crystalline basement during K-metasomatism. Moreover, X-ray diffraction of the recrystallized basement was used to identify microcline, epidote, muscovite (Li-bearing), siderophyllite [Li-bearing $KFe^{2+}{}_2Al(Si_2Al_2)O_{10}(OH)_2$], clinochlore, and chalcopyrite. Although it is worth recognizing the limitations of our two-core data set, it appears likely that K-metasomatism played a key role in Li enrichment of the PRA basement and that Li-bearing muscovite and Li-bearing siderophyllite are the major host phases. It is also noteworthy that we did not interrogate muscovite and siderophyllite directly via microanalytical techniques, and future work is needed to separate and analyze these minerals to thoroughly characterize the major host phases of Li.

Sediment Accumulation of Li and Syndepositional Emplacement

The overlying siliciclastics display many of the same trends that have been reported in modern weathering studies illustrating that the fractionation of Li isotopes are controlled by the balance between primary mineral dissolution and secondary mineral formation—a process known as the weathering congruency (Misra and Froelich, 2012; Pogge von Strandmann and Henderson, 2015). As mentioned in the lithium isotopes background section, primary minerals dissolve without notable fractionation. Secondary minerals preferentially retain ^{6}Li, dictating the isotopic values of water-rock interactions (Huh et al., 1998, 2001; Pistiner and Henderson, 2003; Vigier et al., 2009; Wimpenny et al., 2010). If a rock dissolves congruently without forming secondary minerals, then both the sediment and water will have δ^7Li values approximately equal to the parent rock (Pogge von Strandmann et al., 2020). In contrast, incongruent dissolution of minerals is characterized by secondary mineral formation, which results in greater Li isotopic differences between sediment and water, where sediments are enriched in ^{6}Li and waters are enriched in ^{7}Li (Misra and Froelich, 2012). This behavior during weathering enables Li to be used as a tracer for silicate weathering processes (Dellinger et al., 2015).

Regolith directly overlying the recrystallized basement (109.8 ppm, 5.9‰) shows a minor decrease in Li content (94.0 ppm) and a more positive δ^7Li value (8.5‰). This is interpreted to be the result of early mineral dissolution preceding the accumulation of significant abundances of secondary minerals (i.e., congruent dissolution) leading to a δ^7Li value near that of the source rock, and the leaching of dissolved Li basinward by meteoric waters. Pebbly to coarse-grained channel sandstones of Facies 3 exhibit some of the isotopically heaviest and Li-depleted sediments (6.2‰–23.5‰; 2.1–36.5 ppm). This is attributed to the high mechanical energy and short residence time in a braided fluvial system. Fine-grained alteration minerals produced during chemical weathering in such high energy systems are more likely to bypass deposition and the resulting paucity of secondary minerals would therefore prevent the accumulation of ^{6}Li leading to δ^7Li values within the river that are more reflective of its waters. As evidenced in the surrounding floodplain deposits of Facies 4, extensive paleosols formed along the banks of these channels: X-ray diffraction results show that these sediments are composed of quartz, microcline, orthoclase, muscovite, and kaolinite. As expected, the formation of clay minerals in these paleosols lead them to be isotopically light (δ^7Li = 1.5‰–8.1‰) and these deposits host the greatest bulk Li concentrations recorded in this study (28.2–167.3 ppm; Fig. 5). Within Facies 4, kaolinite and muscovite are interpreted to be the major host phases of Li, and fluctuations in their concentration are ascribed to varying sources of weathered regolith and soil forming processes.

Interestingly, all three cores are located on the subaerially exposed drainage of the PRA, and despite being as much as 150 km away from each other, the maximum concentration of Li in paleosol samples reached similar values (166.4 ppm, 167.3 ppm, and 109.4 ppm; Table 2). This suggests that the intensity of weathering across the arch remained similar, and if correct, it can be reasoned that these probably represent the Li carrying capacity of paleosols that formed along the flanks. This, however, raises questions regarding the weathering intensity and carrying capacity of sediments located along the crest of the PRA. Numerous studies have shown that the PRA is riddled with fault-bounded grabens and other paleotopographic lows owing to the extensive nature of its formation, and these regions have accumulated up to 100 m of Granite Wash sediments (Cant, 1988; Trotter, 1989; Dec et al., 1996; Balshaw, 2010; Fig. 1). Although still speculative, it is possible that these comparatively stable sub-basins host larger volumes and higher concentrations of Li-enriched sediments. This could be due to basement sources with greater Li concentrations, or overall lower erosion rates, which may have allowed for more intense weathering and potentially greater Li-carrying capacity compared to sediments located along the basin's limbs. By contrast, evidence for congruent dissolution of minerals suggests that, at the highest levels of weathering intensity, secondary minerals hosting Li break down and the Li is leached into surrounding waters (Dellinger et al., 2015). This decrease in Li abundance is observed in paleosol samples D-008 and D-009 as well as D-010 and D-011 (Fig. 4). In both cases, samples were taken at the base and near the top of the paleosol bed, and while their δ^7Li values remained similar within error, the samples taken up-section contained less than 50% of the amount of Li in the lower sample (Table 2). If more intensely weathered sediments exist along the crest of the arch, it is reasonable to assume these same processes occurred. However, even if these sediments are weathered to such an extent that Li has now been leached out, considering that many of these sub-basins remained relatively isolated from drainage into the surrounding WCSB, they may represent localized regions of greater Li enrichment. As such, isolated, fault-bounded grabens filled with Granite Wash sediments represent an intriguing target of future study in understanding the extent of weathering intensity and Li accumulation along the crest of the PRA.

Facies 8 and 9 siliciclastics of the Gilwood Member display many of the same trends exemplified by the Granite Wash (Fig. 5). Medium-grained sandstones of the delta front generally show low Li concentrations and high δ^7Li values, whereas heterolithic sediments characterized by flaser and wavy bedding distinctly show lower δ^7Li values and higher Li concentrations. Prodeltaic, bioturbated silty sandstones of Facies 9 exhibit a narrow range of low δ^7Li values and, aside from a single sample, moderate to high Li concentrations (Fig. 5). Much like the Granite Wash, these variations are ascribed to the proportion of secondary clay minerals within the sediments. Although Gilwood Member sediments display Li isotopic signatures similar to the Granite Wash, they notably contain lower Li concentrations (Fig. 5). Early characterizations of the Gilwood Member show that these sediments are similar to those of the Granite Wash, but are texturally and mineralogically more mature (Shawa, 1969). This is because the Gilwood Member is at least a second order deposit of Granite Wash sediments, which were reworked along the coastal plain following a regressive phase in the Middle Devonian

(Shawa, 1969). Our results support this interpretation, and we attribute the lower Li concentrations to losses of Li during sediment transport and reworking that increased sediment maturity.

The remaining evaporitic, carbonate, and brackish to freshwater mudstones of Facies 5, 6, 10, and 11 generally have higher δ^7Li values and very low Li concentrations (Fig. 5). These sediments were all deposited under various subaqueous conditions and are interpreted to reflect their local hydrochemistry and depositional environment. Dolomitic mudstones of the restricted lagoon are extremely Li depleted and isotopically heavy (0.4 ppm; 22.0‰) because Li does not readily incorporate into carbonate phases (Burton and Vigier, 2012), and the nearshore lagoons from which they were deposited were highly influenced by the ^{7}Li-enriched river waters draining the PRA. The deep lagoon laminates of Facies 6 display equally low Li concentrations. However, they are isotopically much lighter (1.4 ppm; 6.7‰), comparable with paleosols on the PRA. These values are attributed to the suspension settling of isotopically light clay minerals in the deep lagoon, because as in carbonate minerals, Li does not readily accumulate in evaporitic minerals (Mertineit and Schramm, 2019). These findings are consistent with those of Sarchi et al. (2023), who examined Li-rich brines in the salars of Argentina and found that even under extreme evaporative conditions, dissolved Li remained in solution and concentrated in the residual brine.

Although primary carbonates can be a reliable archive of paleoseawater chemistry (Kalderon-Asael et al., 2021), various diagenetic processes are known to influence carbonate geochemistry and can result in Li isotope ratios that are unrelated to seawater composition (Brand and Veizer, 1980; Swart, 2015; Dellinger et al., 2020). Marine burial diagenesis may reset the δ^7Li value of carbonate rocks to the composition of marine water with little variability (Dellinger et al., 2020). By contrast, meteoric diagenesis may impart highly variable δ^7Li signatures that are wholly unrelated to the original composition and have been shown to impart δ^7Li values up to 9‰ ± 4‰ lighter than seawater composition (Dellinger et al., 2020). The platform carbonates of Facies 10 show low concentrations of Li (0.4–2.8 ppm) and variable δ^7Li values (10.4‰–16.8‰), which we interpret, at least in part, as post-depositional overprinting by meteoric diagenesis.

Blocky mudstones of Facies 11 show similarly low Li concentrations (3.1–5.6 ppm) and relatively heavy δ^7Li values (16.4‰–19.6‰), which we interpret to reflect the isotopic composition of their brackish to freshwater subaqueous conditions.

Implications for Li Brines in the WCSB and Deep Sedimentary Basins Globally

The aim of this discussion is not to resolve the evolution of deep groundwater brines in the WCSB. Rather, it is an initial effort to identify the origins of Li in the WCSB and demonstrate the greater potential of Li isotopes for identifying the genesis and distribution of Li in deep-time contexts. By examining when and where it was deposited in relation to the basin's evolution, we offer a new perspective on the processes of Li cycling and enrichment in deep sedimentary basins globally.

Figure 6 outlines the Li concentrations of brines sampled across Alberta and Saskatchewan overlain with the locations of the PRA, West Alberta Ridge, and the approximate boundary of the Athabasca Mobile Zone (modified from Drees et al, 1994; Burwash and Krupička, 1970; Reimert et al., 2022; Government of Saskatchewan, 2023). It was previously recognized that within the Alberta basin, the highest Li concentrations (≤140 mg/L) exist within formation waters of west-central Devonian strata (Givetian and Frasnian) (Hitchon et al., 1993; Eccles and Berhane, 2011; Lyster et al., 2022). This is similarly observed in Saskatchewan, where elevated Li concentrations are observed within the respective Givetian and Frasnian aged Winnipegosis and Duperow formations (Jensen, 2015, 2016; Jensen and Rostron, 2018). The highest Li concentrations occur on the PRA or along a zone that approximately parallels the West Alberta Ridge trending southeast into central Alberta. Although the complex hydrochemical evolution of formation waters within the WCSB is beyond the scope of this discussion, a few notable trends have emerged in this study.

Li brines in west-central Alberta are correlated with enriched ^{87}Sr/^{86}Sr levels, whereas those from central Alberta show the influence from the evaporation-concentration of paleoseawater and the subsequent dissolution of evaporite minerals (Eccles and Berhane, 2011; Huff, 2016, 2019). We suggest that these trends reflect the weathering and accumulation of continental sediments in the surrounding basin and not hydrothermal influxes. Our results imply that crystalline basement of the PRA served as a Li source material through which weathering processes led to its enrichment in overlying siliciclastics of the Granite Wash. These sediments were transported into the surrounding restricted basin syndepositional to its development, and the accumulation of Li was facies dependent, and directly related to the extent of secondary mineral formation. Siliciclastics of the Granite Wash represent a series of freshwater fluvial systems draining the high relief basement structure and have been shown to interfinger in some capacity with every onlapping unit throughout transgression of the Sauk Sequence and until its burial in the Late Devonian (Porter et al., 1982; Keith, 1990; McMechan, 1990; Trotter and Hein, 1988). Much like modern fluvial systems (e.g., Huh et al., 2001; Millot et al., 2010a), rivers draining the PRA carried a suspended load and trace levels of dissolved Li into the restricted basin. We suggest that the enriched ^{87}Sr/^{86}Sr levels observed by Eccles and Berhane (2011) near the PRA reflect the syndepositional emplacement of basement-derived, Li-bearing sediments, rather than post-depositional hydrothermal overprinting.

Eastward into central Alberta and south-central Saskatchewan, seawater evaporation reached extreme levels throughout the Devonian (Fig. 3A; Hauck and Grobe, 2020). Halite precipitation occurs after ∼90% of seawater is evaporated, and as suggested by Huff (2016, 2019), it was this extreme evaporation-concentration of seawater that led to the formation of Li-rich brines in central Alberta. Although the Li concentration of Devonian seawater in the WCSB is not known, modern seawater averages ∼0.18 ppm Li (Penniston-Dorland et al., 2017). It is not difficult to envision the evaporation-concentration of seawater increasing Li to values ranging between 0.1 ppm and 50 ppm: marine circulation was limited during this time (i.e., Hauck and Grobe, 2020) and the basin straddled the equator during the lower Devonian. Lithium was also persistently supplied by fluvial input from within the basin, at least in the area of the PRA. The average concentration of dissolved Li in modern rivers ranges between 0.0001 ppb and 23 ppb (average ∼1.8 ppb), and suspended sediments from contemporary rivers draining the Mackenzie Basin in Canada, for example, show Li concentrations ranging between 17.8 ppm and 57.8 ppm (Tomascak et al., 2016; Millot et al., 2010a). Considering the basin's restricted nature, it is probable that Li sourced from the PRA and transported via river processes complemented the evaporation-concentration of Li in the seawater. We suggest this process to be particularly important toward the southeast, where the basin becomes increasingly evaporative, and age equivalent units comprise thick successions of halite and sylvite. In south-central Saskatchewan, Jensen et al. (2020) observed high Li concentrations in the evaporites and carbonates of the Duperow Formation (≤113 ppm). It seems unlikely that Li-enriched regolith was confined solely to the PRA. The nearby exposed Canadian Shield on the northeast edge of the WCSB is also a likely source.

Lastly, we cannot discount the complex post-depositional processes that led to the evolution

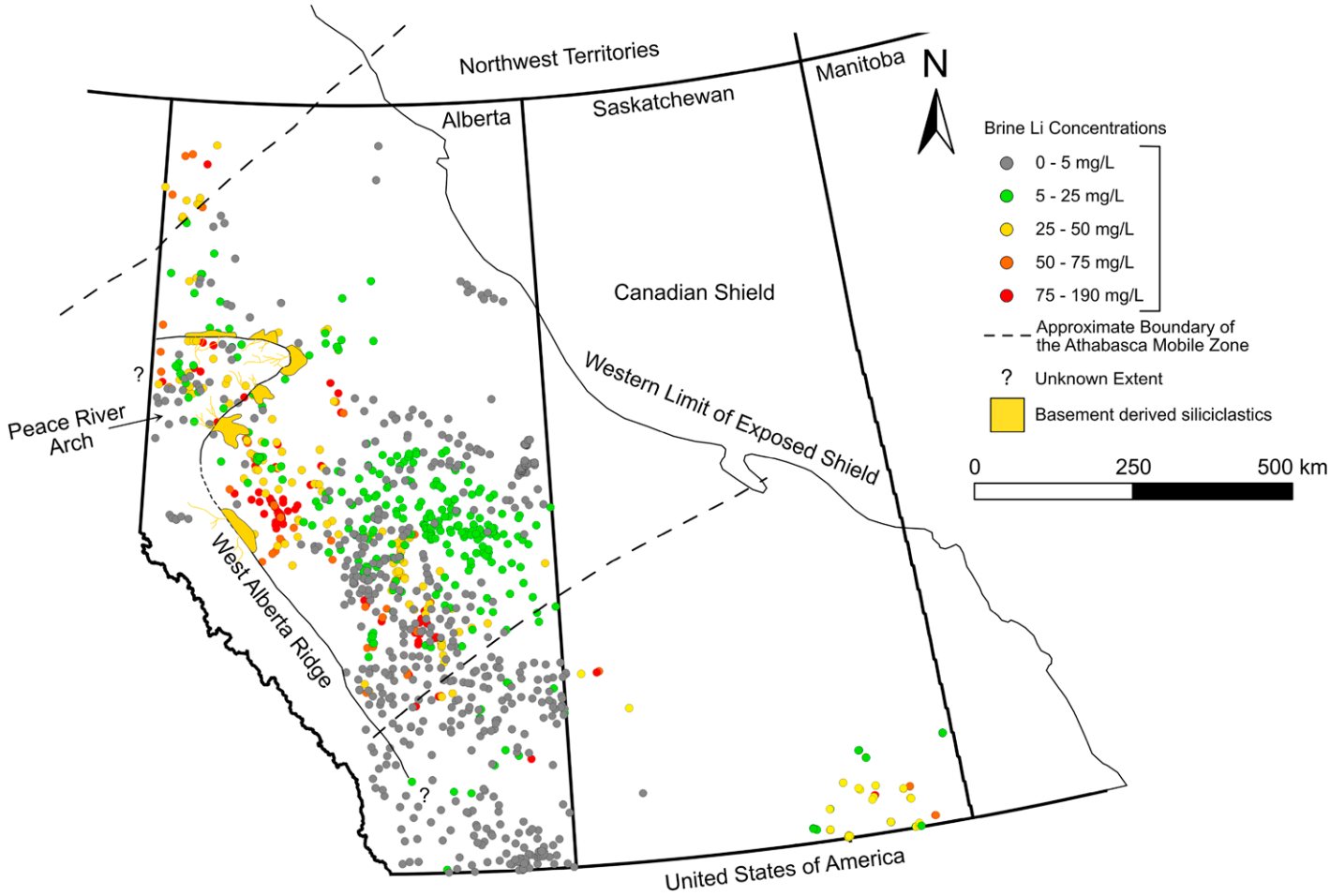

Figure 6. Distribution of Li brines across Alberta and Saskatchewan in relation to the Peace River Arch (PRA) and West Alberta Ridge (modified from Drees et al., 1994). Dashed lines represent the approximate zone of deformation and K-metasomatism as defined by Burwash and Krupička (1970). These are overlain by a schematic depiction of the transportation of Granite Wash sediments. Li-rich sediments derived from the PRA are transported into the basin along prograding fluvial systems. These sediments interfinger with every unit onlapping the PRA until its burial in the Late Devonian (McMechan, 1990). Li brine data are from the respective Alberta Geological Survey (Reimert et al., 2022) and the Government of Saskatchewan (2023) databases.

of formational brines, particularly in the Alberta basin. While we suggest Li emplacement to be syndepositional to development of the basin, and the concentrations of these formational waters seemingly reflect their proximity to the PRA (Fig. 6), the complex water-rock interactions associated with the density driven migration and tectonic flushing of these units undoubtedly played a significant role in the redistribution of Li across the basin (Connolly et al., 1990a, 1990b; Huff, 2016, 2019).

In a global context, Li rich groundwaters have been documented in 48 sedimentary basins worldwide, yet the sources of Li in these brines and timing of emplacement remains elusive (Dugamin et al., 2021; Sanjuan et al., 2022). Current explanations for the formation of these groundwaters focus on reconstructing brine chemistry using some combination of late-stage seawater evaporation, meteoric water mixing, water-rock interactions, or hydrothermal influx (e.g., Connolly et al., 1990a, 1990b; Elders and Cohen, 1983; Wilson and Long, 1993; Stueber et al., 1993; Tesmer et al., 2007; Sanjuan et al., 2022; Dugamin et al., 2023). While these approaches may effectively describe groundwater chemistry, the limited availability of rock data from many deep basins often results in a lack of detailed geological context, leading to reliance on generalized or theoretical scenarios. The WCSB exemplifies these challenges given its complex geological and hydrological history. Previous interpretations of Li enrichment in the basin have primarily been ascribed to hydrothermal fluids exsolving from deep basement fractures, with secondary contributions from seawater evaporation-concentration (Eccles and Berhane, 2011; Huff, 2016, 2019). Our findings suggest that while evaporation-concentration likely played a role, tracing Li to its source requires a robust geological framework of the basin.

Modern rivers, estimated to account for ~50% of Li input into the oceans (Hathorne and James, 2006), have generally low Li concentrations (~1.8 ppb). However, terrestrial clay minerals contain significantly higher concentrations (~5.0–300 ppm), suggesting that a substantial proportion of Li derived from primary rocks is stored within secondary minerals on the continents (Huh et al., 1998; Tomascak et al., 2016; Pogge von Strandmann et al., 2020). Although continental weathering is known to fluctuate over geological time scales (i.e., Kalderon-Asael et al., 2021), weathering processes represent a significant proportion of mobile Li at Earth's surface (Liu and Rudnick, 2011). Source rocks

with high Li potential, such as volcanic, granitic, and pegmatitic rocks, occur globally, and sediments weathered from these sources accumulate in continental basins where they are buried and preserved. To effectively characterize the Li potential of deep sedimentary basins, it is essential to recognize that weathering processes, both modern and ancient, have played a central role in Li transport at Earth's surface. Understanding the nature and distribution of basin-fill sediments is therefore essential for informing global Li exploration strategies.

CONCLUSIONS

In order to test the prevailing hypotheses for the Li source to the Alberta basin, we examined Precambrian basement rock of the PRA and its overlying siliciclastics, carbonates, and evaporites. We logged the units, divided them into lithofacies, and examined them for their Li isotopic content and Li concentration. The enrichment of Li and its isotopic content in the derived sediments are entirely controlled by the ratio of secondary mineral formation during low temperature weathering processes. We report no evidence of hydrothermal alteration; instead, our results indicate that the Li is derived from crystalline basement of the PRA. It accumulated in overlying sediments and was subsequently transported into the surrounding basin through fluvial processes. We propose that Li enrichment occurred syndepositional to development of the basin, where concurrent evaporation of basinal seawater and continental delivery of Li contributed to its enrichment. Our results highlight a direct link between syndepositional processes and modern dissolved Li concentrations in groundwater. Our approach integrates Li isotopes with sedimentological and hydrogeochemical data to establish a framework for understanding the genesis of Li concentrations in deep-time contexts. This approach can be directly applied to analogous sedimentary basins worldwide, providing valuable insights to guide global Li exploration efforts.

ACKNOWLEDGMENTS

Funding for this research was generously provided by the Natural Sciences and Engineering Research Council of Canada (NSERC) Discovery Grants to M. Gingras (RGPIN-2020-0513) and K. Konhauser (RGPIN-2020-05189). We extend our sincere thanks to Troy Rasbury and Yue Cai for their support in handling our manuscript and Yongjie Lin and two other anonymous reviewers for their valuable and constructive feedback.

REFERENCES CITED

Aitken, J.D., 1971, Control of lower Paleozoic sedimentary facies by the Kicking Horse Rim, Southern Rocky Mountains, Canada: Bulletin of Canadian Petroleum Geology, v. 19, p. 557–569, https://doi.org/10.35767/gscpgbull.19.3.557.

Ambrose, H., and Kendall, A., 2020, Understanding the future of lithium: Part 1, resource model: Journal of Industrial Ecology, v. 24, p. 80–89, https://doi.org/10.1111/jiec.12949.

Araoka, D., Kawahata, H., Takagi, T., Watanabe, Y., Nishimura, K., and Nishio, Y., 2014, Lithium and strontium isotopic systematics in playas in Nevada, USA: Constraints on the origin of lithium: Mineralium Deposita, v. 49, p. 371–379, https://doi.org/10.1007/s00126-013-0495-y.

Balshaw, K.E., 2010, Sedimentology and stratigraphy of the granite wash: Contact rapids and Keg River sandstone (Red Earth Area) [M.S. thesis]: Edmonton, Alberta, Canada, University of Alberta, https://doi.org/10.7939/R3H12VG45.

Benson, T.R., Coble, M.A., Rytuba, J.J., and Mahood, G.A., 2017, Lithium enrichment in intracontinental rhyolite magmas leads to Li deposits in caldera basins: Nature Communications, v. 8, 270, https://doi.org/10.1038/s41467-017-00234-y.

Beaumont, C., Quinlan, G.M., and Stockmal, G.S., 1993, The evolution of the Western Interior Basin: Causes, consequences and unsolved problems, *in* Caldwell, W.G.E., and Kauffman, E.G., eds., Evolution of the Western Interior Basin: Geological Association of Canada, Special Paper 39, p. 97–117.

Benvenuto, G.L., and Price, R.A., 1979, Structural Evolution of the Hosmer Thrust Sheet, Southeastern British Columbia: Bulletin of Canadian Petroleum Geology, v. 27, p. 360–394, https://doi.org/10.35767/gscpgbull.27.3.360.

Bibienne, T., Magnan, J.-F., Rupp, A., and Laroche, N., 2020, From mine to mind and mobiles: Society's increasing dependence on lithium: Elements, v. 16, p. 265–270, https://doi.org/10.2138/gselements.16.4.265.

Bond, G.C., and Kominz, M.A., 1984, Construction of tectonic subsidence curves for the early Paleozoic miogeocline, southern Canadian Rocky Mountains: Implications for subsidence mechanisms, age of breakup, and crustal thinning: Geological Society of America Bulletin, v. 95, p. 155–173, https://doi.org/10.1130/0016-7606(1984)95<155:COTSCF>2.0.CO;2.

Bowell, R.J., Lagos, L., de los Hoyos, C.R., and Declercq, J., 2020, Classification and characteristics of natural lithium resources: Elements, v. 16, p. 259–264, https://doi.org/10.2138/gselements.16.4.259.

Brand, U., and Veizer, J., 1980, Chemical diagenesis of a multicomponent carbonate system; l, Trace elements: Journal of Sedimentary Research, v. 50, p. 1219–1236, https://doi.org/10.1306/212F7BB7-2B24-11D7-8648000102C1865D.

Breunig, H.M., Birkholzer, J.T., Borgia, A., Oldenburg, C.M., Price, P.N., and McKone, T.E., 2013, Regional evaluation of brine management for geologic carbon sequestration: International Journal of Greenhouse Gas Control, v. 14, p. 39–48, https://doi.org/10.1016/j.ijggc.2013.01.003.

Burton, K.W., and Vigier, N., 2012, Lithium isotopes as tracers in marine and terrestrial environments, *in* Baskaran, M., ed., Handbook of Environmental Isotope Geochemistry: Berlin, Heidelberg, Spinger, p. 41–59, https://doi.org/10.1007/978-3-642-10637-8_4.

Burwash, R.A., and Krupička, J., 1969, Cratonic reactivation in the Precambrian basement of western Canada. I. Deformation and chemistry: Canadian Journal of Earth Sciences, v. 6, p. 1381–1396, https://doi.org/10.1139/e69-140.

Burwash, R.A., and Krupička, J., 1970, Cratonic reactivation in the Precambrian basement of western Canada: Part II—Metasomatism and isostasy: Canadian Journal of Earth Sciences, v. 7, p. 1275–1294, https://doi.org/10.1139/e70-120.

Burwash, R.A., Chacko, T., Muehlenbachs, K., and Bouzidi, Y., 2000, Oxygen isotope systematics of the Precambrian basement of Alberta: Implications for Paleoproterozoic and Phanerozoic tectonics in northwestern Alberta: Canadian Journal of Earth Sciences, v. 37, p. 1611–1628, https://doi.org/10.1139/e00-090.

Cant, D.J., 1988, Regional structure and development of the Peace River Arch, Alberta: A Paleozoic failed-rift system?: Bulletin of Canadian Petroleum Geology, v. 36, p. 284–295, https://doi.org/10.35767/gscpgbull.36.3.284.

Chan, L.H., Edmond, J.M., Thompson, G., and Gillis, K., 1992, Lithium isotopic composition of submarine basalts: Implications for the lithium cycle in the oceans: Earth and Planetary Science Letters, v. 108, p. 151–160, https://doi.org/10.1016/0012-821X(92)90067-6.

Chan, L.H., Edmond, J.M., and Thompson, G., 1993, A lithium isotope study of hot springs and metabasalts from mid-ocean ridge hydrothermal systems: Journal of Geophysical Research: Solid Earth, v. 98, no. B6, p. 9653–9659, https://doi.org/10.1029/92JB00840.

Chan, L.H., Gieskes, J.M., Chen-Feng, Y., and Edmond, J.M., 1994, Lithium isotope geochemistry of sediments and hydrothermal fluids of the Guaymas Basin, Gulf of California: Geochimica et Cosmochimica Acta, v. 58, p. 4443–4454, https://doi.org/10.1016/0016-7037(94)90346-8.

Chan, L.H., Leeman, W.P., and Plank, T., 2006, Lithium isotopic composition of marine sediments: Geochemistry, Geophysics, Geosystems, v. 7, https://doi.org/10.1029/2005GC001202.

Clergue, C., Dellinger, M., Buss, H.L., Gaillardet, J., Benedetti, M.F., and Dessert, C., 2015, Influence of atmospheric deposits and secondary minerals on Li isotopes budget in a highly weathered catchment, Guadeloupe (Lesser Antilles): Chemical Geology, v. 414, p. 28–41, https://doi.org/10.1016/j.chemgeo.2015.08.015.

Coffey, D.M., Munk, L.A., Ibarra, D.E., Butler, K.L., Boutt, D.F., and Jenckes, J., 2021, Lithium storage and release from lacustrine sediments: Implications for lithium enrichment and sustainability in continental brines: Geochemistry, Geophysics, Geosystems, v. 22, https://doi.org/10.1029/2021GC009916.

Connolly, C.A., Walter, L.M., Baadsgaard, H., and Longstaffe, F.J., 1990a, Origin and evolution of formation waters, Alberta Basin, Western Canada sedimentary Basin. I. Chemistry: Applied Geochemistry, v. 5, p. 375–395, https://doi.org/10.1016/0883-2927(90)90016-X.

Connolly, C.A., Walter, L.M., Baadsgaard, H., and Longstaffe, F.J., 1990b, Origin and evolution of formation waters, Alberta Basin, Western Canada Sedimentary Basin. II. Isotope systematics and water mixing: Applied Geochemistry, v. 5, p. 397–413, https://doi.org/10.1016/0883-2927(90)90017-Y.

Dec, T., Hein, F.J., and Trotter, R.J., 1996, Granite wash alluvial fans, fan-deltas and tidal environments, northwestern Alberta: Implications for controls on distribution of Devonian clastic wedges associated with the Peace River Arch: Bulletin of Canadian Petroleum Geology, v. 44, p. 541–565, https://doi.org/10.35767/gscpgbull.44.3.541.

Dellinger, M., Gaillardet, J., Bouchez, J., Calmels, D., Louvat, P., Dosseto, A., Gorge, C., Alanoca, L., and Maurice, L., 2015, Riverine Li isotope fractionation in the Amazon River basin controlled by the weathering regimes: Geochimica et Cosmochimica Acta, v. 164, p. 71–93, https://doi.org/10.1016/j.gca.2015.04.042.

Dellinger, M., Hardisty, D.S., Planavsky, N.J., Gill, B.C., Kalderon-Asael, B., Asael, D., Croissant, T., Swart, P.K., and West, A.J., 2020, The effects of diagenesis on lithium isotope ratios of shallow marine carbonates: American Journal of Science, v. 320, p. 150–184, https://doi.org/10.2475/02.2020.03.

Donaldson, W.S., Plint, A.G., and Longstaffe, F.J., 1999, Tectonic and eustatic control on deposition and preservation of Upper Cretaceous ooidal ironstone and associated facies: Peace River Arch area, NW Alberta, Canada: Sedimentology, v. 46, p. 1159–1182, https://doi.org/10.1046/j.1365-3091.1999.00271.x.

Drees, N.C.M., Mossop, G.D., and Shetsen, I., 1994, Devonian Elk point group of the western Canada sedimentary basin, *in* Mossop, G.D., and Shetsen, I., compilers, Geological Atlas of the Western Canada Sedimentary Basin: Alberta Geological Survey, v. 4, p. 129–138.

Dugamin, E.J.M., Richard, A., Cathelineau, M., Boiron, M.-C., Despinois, F., and Brisset, A., 2021, Groundwater in sedimentary basins as potential lithium resource: A global prospective study: Scientific Reports, v. 11, 21091, https://doi.org/10.1038/s41598-021-99912-7.

Dugamin, E.J.M., Cathelineau, M., Boiron, M.C., Richard, A., and Despinois, F., 2023, Lithium enrichment pro-

cesses in sedimentary formation waters: Chemical Geology, v. 635, https://doi.org/10.1016/j.chemgeo.2023.121626.

Eccles, D.R., and Berhane, H., 2011, Geological Introduction to Lithium-Rich Formation Water with Emphasis on the Fox Creek Area of West-Central Alberta (NTS 83F and 83 K): Energy Resources Conservation Board, Alberta Geological Survey Open-File Report 2011-10, 22 p., https://ags.aer.ca/publications/all-publications/ofr-2011-10.

Elders, W.A., and Cohen, L.H., 1983, The Salton Sea Geothermal Field, California, as a near-field natural analog of a radioactive waste repository in salt: U.S. Department of Energy, Technical Report, 138 p., https://doi.org/10.2172/5585044.

Godfrey, L., and Álvarez-Amado, F., 2020, Volcanic and saline lithium inputs to the Salar de Atacama: Minerals (Basel), v. 10, 201, https://doi.org/10.3390/min10020201.

Government of Saskatchewan, 2023, Chemistry of Produced Formation Waters from Oil Wells in Saskatchewan: Government of Saskatchewan Dataset, https://geohub.saskatchewan.ca/datasets/saskatchewan::chemistry-of-produced-formation-waters-from-oil-wells-in-saskatchewan/about (accessed May 2025).

Hathorne, E., and James, R., 2006, Temporal record of lithium in seawater: A tracer for silicate weathering?: Earth and Planetary Science Letters, v. 246, p. 393–406, https://doi.org/10.1016/j.epsl.2006.04.020.

Hauck, T.E., 2014, Regional Correlation of the Beaverhill Lake Group in the Subsurface of Alberta, Townships 29 to 113 and Ranges 1W4 to 13W6: Alberta Energy Regulator, Alberta Geological Survey, AER/AGS Open-File Report 2014-05, 29 p., https://ags.aer.ca/publications/all-publications/ofr-2014-05.

Hauck, T.E., and Grobe, M., 2020, Upper Elk Point subgroup paleogeography and evaporite distribution with implications for evaporite dissolution, karstification, and carbonate diagenesis in northeastern Alberta: Bulletin of Canadian Petroleum Geology, v. 68, p. 91–122, https://doi.org/10.35767/gscpgbull.68.4.91.

Hitchon, B., Bachu, S., and Underschultz, J., 1993, Industrial Mineral Potential of Alberta Formation Waters: Alberta Research Council, Alberta Geological Survey, ARC/AGS Open-File Report 1993-15, 92 p., https://ags.aer.ca/publications/all-publications/ofr-1993-15.

Huff, G.F., 2016, Evolution of Li-enriched oilfield brines in Devonian carbonates of the south-central Alberta Basin, Canada: Bulletin of Canadian Petroleum Geology, v. 64, p. 438–448, https://doi.org/10.2113/gscpgbull.64.3.438.

Huff, G.F., 2019, Origin and Li-Enrichment of Selected Oilfield Brines in the Alberta Basin, Canada: Alberta Energy Regulator, Alberta Geological Survey, AER/AGS Open File Report 2019-01, 29 p., https://ags.aer.ca/publications/all-publications/ofr-2019-01.

Huh, Y., Chan, L.-H., Zhang, L., and Edmond, J.M., 1998, Lithium and its isotopes in major world rivers: Implications for weathering and the oceanic budget: Geochimica et Cosmochimica Acta, v. 62, p. 2039–2051, https://doi.org/10.1016/S0016-7037(98)00126-4.

Huh, Y., Chan, L.-H., and Edmond, J.M., 2001, Lithium isotopes as a probe of weathering processes: Orinoco River: Earth and Planetary Science Letters, v. 194, p. 189–199, https://doi.org/10.1016/S0012-821X(01)00523-4.

Jansa, L.F., and Fischbuch, N.R., 1974, Evolution of a Middle and Upper Devonian sequence from a clastic coastal plain—Deltaic complex into overlying carbonate reef complexes and banks, Sturgeon-Mitsue area, Alberta: Geological Survey of Canada Bulletin 234, 117 p., https://doi.org/10.4095/103477.

Jeffcoate, A.B., Elliott, T., Thomas, A., and Bouman, C., 2004, Precise/small sample size determinations of lithium isotopic compositions of geological reference materials and modern seawater by MC-ICP-MS: Geostandards and Geoanalytical Research, v. 28, p. 161–172, https://doi.org/10.1111/j.1751-908X.2004.tb01053.x.

Jensen, G.K.S., 2015, Trace element and other analyses of Paleozoic-aged brines from southeastern Saskatchewan (Townships 1 to 13, Ranges 5 to 21 W2 M): Saskatchewan Ministry of the Economy, Saskatchewan Geological Survey Data File 37, https://publications.saskatchewan.ca/#/products/79894.

Jensen, G.K.S., 2016, Results from the 2016 field season for the brine sampling project: Investigating the mineral potential of brines in Saskatchewan, *in* Summary of Investigations 2016, Volume 1, Saskatchewan Geological Survey, Saskatchewan Ministry of the Economy, Miscellaneous Report 20164.1, Paper A-3, 7 p.

Jensen, G.K.S., and Rostron, B.J., 2018, Investigating the mineral potential of brines in Saskatchewan: New results from the brine sampling project for 2018, *in* Summary of Investigations 2018, Volume 1, Saskatchewan Geological Survey, Saskatchewan Ministry of Energy and Resources Miscellaneous Report 2018-4.1, Paper A-5, 8 p., https://publications.saskatchewan.ca/#/products/100657.

Jensen, G.K.S., Pollard, A., and Rostron, B.J., 2020, Lithium concentration in the Duperow Formation: Preliminary results of geochemical analysis of core samples from two wells in southeastern Saskatchewan, *in* Summary of Investigations 2020, Volume 1, Saskatchewan Geological Survey, Saskatchewan Ministry of Energy and Resources Miscellaneous Report 2020-4.1, Paper A-2, 8 p. and 1 appendix, https://publications.saskatchewan.ca/#/products/106648.

Jeppson, D.W., Ballif, J.L., Yuan, W.W., and Chou, B.E., 1978, Lithium literature review: Lithium's properties and interactions: Hanford Engineering Development Laboratory HEDL-TME-78-1.

Kalderon-Asael, B., et al., 2021, A lithium-isotope perspective on the evolution of carbon and silicon cycles: Nature, v. 595, p. 394–398, https://doi.org/10.1038/s41586-021-03612-1.

Keith, W.J., 1990, The influence of the Peace River Arch on Beaverhill Lake sedimentation, *in* O'Connell, S.C., and Bell, J.S., eds., Geology of the Peace River Arch: Bulletin of Canadian Petroleum Geology, v. 38A, p. 55–65, https://doi.org/10.35767/gscpgbull.38a.1.055.

Kharaka, Y.K., and Hanor, J.S., 2003, Deep Fluids in the Continents: I. Sedimentary Basins, *in* Holland, H.D., and Turekian, K.K., eds., Treatise on Geochemistry: Elsevier, v. 5, p. 1–48, https://doi.org/10.1016/B0-08-043751-6/05085-4.

Lemarchand, E., Chabaux, F., Vigier, N., Millot, R., and Pierret, M.-C., 2010, Lithium isotope systematics in a forested granitic catchment (Strengbach, Vosges Mountains, France): Geochimica et Cosmochimica Acta, v. 74, p. 4612–4628, https://doi.org/10.1016/j.gca.2010.04.057.

Li, W., Liu, X.-M., and Chadwick, O.A., 2020, Lithium isotope behavior in Hawaiian regoliths: Soil-atmosphere-biosphere exchanges: Geochimica et Cosmochimica Acta, v. 285, p. 175–192, https://doi.org/10.1016/j.gca.2020.07.012.

Liu, X., and Rudnick, R.L., 2011, Constraints on continental crustal mass loss via chemical weathering using lithium and its isotopes: Proceedings of the National Academy of Sciences of the United States of America, v. 108, p. 20,873–20,880, https://doi.org/10.1073/pnas.1115671108.

Lyster, S., Hauck, T.E., Lopez, G.P., Playter, T.L., Reimert, C., Palombi, D., and Schultz, S.K., 2022, Lithium and Helium in Alberta: Data Compilation and Preliminary Observations: Alberta Energy Regulator, Alberta Geological Survey, AER/AGS Open File Report 2021-04, 36 p., https://ags.aer.ca/publications/all-publications/ofr-2021-04.

Lund, J.W., and Toth, A.N., 2021, Direct utilization of geothermal energy 2020 worldwide review: Geothermics, v. 90, https://doi.org/10.1016/j.geothermics.2020.101915.

Maloney, K.O., and Yoxtheimer, D.A., 2012, Production and disposal of waste materials from gas and oil extraction from the Marcellus Shale Play in Pennsylvania: Environmental Practice, v. 14, p. 278–287, https://doi.org/10.1017/S146604661200035X.

Marschall, H.R., Wanless, V.D., Shimizu, N., Pogge Von Strandmann, P.A.E., Elliott, T., and Monteleone, B.D., 2017, The boron and lithium isotopic composition of mid-ocean ridge basalts and the mantle: Geochimica et Cosmochimica Acta, v. 207, p. 102–138, https://doi.org/10.1016/j.gca.2017.03.028.

Marza, M., Ferguson, G., Thorson, J., Barton, I., Kim, J.H., Ma, L., and McIntosh, J., 2024, Geological controls on lithium production from basinal brines across North America: Journal of Geochemical Exploration, v. 257, https://doi.org/10.1016/j.gexplo.2023.107383.

McMechan, M.E., 1990, Upper Proterozoic to Middle Cambrian history of the Peace River Arch: Evidence from the Rocky Mountains, *in* O'Connell, S.C., and Bell, J.S., eds., Geology of the Peace River Arch: Bulletin of Canadian Petroleum Geology, v. 38A, p. 36–44, https://doi.org/10.35767/gscpgbull.38a.1.036.

Mertineit, M., and Schramm, M., 2019, Lithium occurrences in brines from two German salt deposits (Upper Permian) and first results of leaching experiments: Minerals (Basel), v. 9, p. 766, https://doi.org/10.3390/min9120766.

Millot, R., Scaillet, B., and Sanjuan, B., 2010a, Lithium isotopes in island arc geothermal systems: Guadeloupe, Martinique (French West Indies) and experimental approach: Geochimica et Cosmochimica Acta, v. 74, p. 1852–1871, https://doi.org/10.1016/j.gca.2009.12.007.

Millot, R., Vigier, N., and Gaillardet, J., 2010b, Behaviour of lithium and its isotopes during weathering in the Mackenzie Basin, Canada: Geochimica et Cosmochimica Acta, v. 74, p. 3897–3912, https://doi.org/10.1016/j.gca.2010.04.025.

Misra, S., and Froelich, P.N., 2012, Lithium isotope history of Cenozoic seawater: Changes in silicate weathering and reverse weathering: Science, v. 335, p. 818–823, https://doi.org/10.1126/science.1214697.

Moore, P.F., 1989, The Kaskaskia Sequence: Reefs, platforms and foredeeps—The Lower Kaskaskia Sequence—Devonian, *in* Ricketts, B.D., ed., The Western Canadian Sedimentary Basin—A Case History: Calgary, Alberta, Canadian Society of Petroleum Geologists Special Publication 30, p. 139–164.

Murdock, B.E., Toghill, K.E., and Tapia-Ruiz, N., 2021, A perspective on the sustainability of cathode materials used in lithium-ion batteries: Advanced Energy Materials, v. 11, https://doi.org/10.1002/aenm.202102028.

O'Connell, S.C., Dix, G.R., and Barclay, J.E., 1990, The origin, history, and regional structural development of the Peace River Arch, Western Canada, *in* O'Connell, S.C., and Bell, J.S., eds., Geology of the Peace River Arch: Bulletin of Canadian Petroleum Geology, v. 38A, p. 4–24, https://doi.org/10.35767/gscpgbull.38a.1.004.

Penniston-Dorland, S., Liu, X.-M., and Rudnick, R.L., 2017, Lithium isotope geochemistry: Reviews in Mineralogy and Geochemistry, v. 82, p. 165–217, https://doi.org/10.2138/rmg.2017.82.6.

Pistiner, J.S., and Henderson, G.M., 2003, Lithium-isotope fractionation during continental weathering processes: Earth and Planetary Science Letters, v. 214, p. 327–339, https://doi.org/10.1016/S0012-821X(03)00348-0.

Pogge von Strandmann, P.A.E., and Henderson, G.M., 2015, The Li isotope response to mountain uplift: Geology, v. 43, p. 67–70, https://doi.org/10.1130/G36162.1.

Pogge von Strandmann, P.A.E., Burton, K.W., Opfergelt, S., Eiríksdóttir, E.S., Murphy, M.J., Einarsson, A., and Gislason, S.R., 2016, The effect of hydrothermal spring weathering processes and primary productivity on lithium isotopes: Lake Myvatn, Iceland: Chemical Geology, v. 445, p. 4–13, https://doi.org/10.1016/j.chemgeo.2016.02.026.

Pogge von Strandmann, P.A.E., Frings, P.J., and Murphy, M.J., 2017, Lithium isotope behaviour during weathering in the Ganges Alluvial Plain: Geochimica et Cosmochimica Acta, v. 198, p. 17–31, https://doi.org/10.1016/j.gca.2016.11.017.

Pogge von Strandmann, P.A.E., Fraser, W.T., Hammond, S.J., Tarbuck, G., Wood, I.G., Oelkers, E.H., and Murphy, M.J., 2019, Experimental determination of Li isotope behaviour during basalt weathering: Chemical Geology, v. 517, p. 34–43, https://doi.org/10.1016/j.chemgeo.2019.04.020.

Pogge von Strandmann, P.A.E., Kasemann, S.A., and Wimpenny, J.B., 2020, Lithium and lithium isotopes in Earth's surface cycles: Elements, v. 16, p. 253–258, https://doi.org/10.2138/gselements.16.4.253.

Porter, J.W., Price, R.A., and McCrossan, R.G., 1982, The Western Canada Sedimentary Basin: Philosophical

Transactions of the Royal Society of London, Series A: Mathematical, Physical and Engineering Sciences, v. 305, p. 169–192, https://doi.org/10.1098/rsta.1982.0032.

Qiu, L., Rudnick, R.L., McDonough, W.F., and Merriman, R.J., 2009, Li and δ^7Li in mudrocks from the British Caledonides: Metamorphism and source influences: Geochimica et Cosmochimica Acta, v. 73, p. 7325–7340, https://doi.org/10.1016/j.gca.2009.08.017.

Reimert, C., Lyster, S., Hauck, T.E., Palombi, D., Playter, T.L., Lopez, G.P., and Schultz, S.K., 2022, Water geochemical data, Lithium Prospectivity Project, 2021 (tabular data, tab delimited format): Alberta Energy Regulator/Alberta Geological Survey, AER/AGS Digital Data 2021-0022, https://ags.aer.ca/publications/all-publications/dig-2021-0022.

Romer, R.L., Meixner, A., and Hahne, K., 2014, Lithium and boron isotopic composition of sedimentary rocks—The role of source history and depositional environment: A 250 Ma record from the Cadomian orogeny to the Variscan orogeny: Gondwana Research, v. 26, p. 1093–1110, https://doi.org/10.1016/j.gr.2013.08.015.

Sanjuan, B., Gourcerol, B., Millot, R., Rettenmaier, D., Jeandel, E., and Rombaut, A., 2022, Lithium-rich geothermal brines in Europe: An up-date about geochemical characteristics and implications for potential Li resources: Geothermics, v. 101, https://doi.org/10.1016/j.geothermics.2022.102385.

Sarchi, C., Lucassen, F., Meixner, A., Caffe, P.J., Becchio, R., and Kasemann, S.A., 2023, Lithium enrichment in the Salar de Diablillos, Argentina, and the influence of Cenozoic volcanism in a basin dominated by Paleozoic basement: Mineralium Deposita, v. 58, p. 1351–1370, https://doi.org/10.1007/s00126-023-01181-z.

Shawa, M.S., 1969, Sedimentary history of the Gilwood Sandstone (Devonian) Utikuma Lake Area, Alberta, Canada: Bulletin of Canadian Petroleum Geology, v. 17, p. 392–409, https://doi.org/10.35767/gscpgbull.17.4.392.

Sikabonyi, L.A., and Rodgers, W.J., 1959, Paleozoic tectonics and sedimentation in the northern half of the West Canadian Basin: Journal of the Alberta Society of Petroleum Geologists, v. 7, no. 9, p. 193–216.

Steinhoefel, G., Brantley, S.L., and Fantle, M.S., 2021, Lithium isotopic fractionation during weathering and erosion of shale: Geochimica et Cosmochimica Acta, v. 295, p. 155–177, https://doi.org/10.1016/j.gca.2020.12.006.

Stelck, C.R., 1975, Basement control of Cretaceous sand sequences in Western Canada, *in* Caldwell, W.G.E, ed., The Cretaceous System in the Western Interior of North America: Geological Association of Canada Special Paper 13, p. 427–440.

Stelck, C.R., Burwash, R.A., and Stelck, D.R., 1978, The Vreeland High: A Cordilleran expression of the Peace River Arch: Bulletin of Canadian Petroleum Geology, v. 26, p. 87–104, https://doi.org/10.35767/gscpgbull.26.1.087.

Stueber, A.M., Walter, L.M., Huston, T.J., and Pushkar, P., 1993, Formation waters from Mississippian-Pennsylvanian reservoirs, Illinois basin, USA: Chemical and isotopic constraints on evolution and migration: Geochimica et Cosmochimica Acta, v. 57, p. 763–784, https://doi.org/10.1016/0016-7037(93)90167-U.

Swart, P.K., 2015, The geochemistry of carbonate diagenesis: The past, present and future: Sedimentology, v. 62, p. 1233–1304, https://doi.org/10.1111/sed.12205.

Teng, F.-Z., McDonough, W.F., Rudnick, R.L., Dalpé, C., Tomascak, P.B., Chappell, B.W., and Gao, S., 2004, Lithium isotopic composition and concentration of the upper continental crust: Geochimica et Cosmochimica Acta, v. 68, p. 4167–4178, https://doi.org/10.1016/j.gca.2004.03.031.

Tesmer, M., Moller, P., Wieland, S., Jahnke, C., Voigt, H., and Pekdeger, A., 2007, Deep reaching fluid flow in the North East German Basin: Origin and processes of groundwater salinisation: Hydrogeology Journal, v. 15, p. 1291–1306, https://doi.org/10.1007/s10040-007-0176-y.

Tomascak, P.B., 2004, Developments in the understanding and application of lithium isotopes in the Earth and Planetary Sciences: Reviews in Mineralogy and Geochemistry, v. 55, p. 153–195, https://doi.org/10.2138/gsrmg.55.1.153.

Tomascak, P.B., Magna, T., and Dohmen, R., 2016, Advances in Lithium Isotope Geochemistry: Springer International Publishing, https://doi.org/10.1007/978-3-319-01430-2, 195 p.

Trotter, R., 1989, Sedimentology and depositional setting of the Granite Wash of the Utikuma and Red Earth areas, north-central Alberta [M.Sc. thesis]: Halifax, Nova Scotia, Canada, Dalhousie University, 378 p.

Trotter, R., and Hein, F.J., 1988, Sedimentology and depositional setting of the Granite Wash, Northwestern Alberta, *in* James, D.P., and Leckie, D.A., eds., Sequences, Stratigraphy, Sedimentology: Surface and Subsurface: Canadian Society of Petroleum Geologists Memoir 15, p. 475–484.

USGS (U.S. Geological Survey), 2023, Mineral Commodity Summaries 2023: U.S. Geological Survey, 210 p., https://doi.org/10.3133/mcs2023.

Vigier, N., Gislason, S.R., Burton, K.W., Millot, R., and Mokadem, F., 2009, The relationship between riverine lithium isotope composition and silicate weathering rates in Iceland: Earth and Planetary Science Letters, v. 287, p. 434–441, https://doi.org/10.1016/j.epsl.2009.08.026.

Williams, C.A., 1997, Depositional Dynamics of Middle Devonian Deposits in the Elk Point Basin: Gilwood Member (Watt Mountain Formation), Nipisi Field, Northcentral Alberta and Yahatinda Formation (Rocky Mountain Front Ranges) [Ph.D. thesis]: Calgary, Alberta, Canada, University of Calgary, 463 p., http://hdl.handle.net/1880/26914.

Wilson, T.P., and Long, D.T., 1993, Geochemistry and isotope chemistry of Michigan Basin brines: Devonian formations: Applied Geochemistry, v. 8, p. 81–100, https://doi.org/10.1016/0883-2927(93)90058-O.

Wimpenny, J., Gíslason, S.R., James, R.H., Gannoun, A., Pogge Von Strandmann, P.A.E., and Burton, K.W., 2010, The behaviour of Li and Mg isotopes during primary phase dissolution and secondary mineral formation in basalt: Geochimica et Cosmochimica Acta, v. 74, p. 5259–5279, https://doi.org/10.1016/j.gca.2010.06.028.

Science Editor: Troy Rasbury
Associate Editor: Yue Cai

Manuscript Received 1 November 2024
Revised Manuscript Received 18 April 2025
Manuscript Accepted 20 May 2025